Nano Energy 51 (2018) 408–424

Contents lists available at ScienceDirect

Nano Energy

journal homepage: www.elsevier.com/locate/nanoen

Review

Breakthroughs in NiO_x-HTMs towards stable, low-cost and efficient perovskite solar cells

Sajid Sajid[a], Ahmed Mourtada Elseman[a,b], Hao Huang[a], Jun Ji[a], Shangyi Dou[a], Haoran Jiang[a], Xin Liu[a], Dong Wei[a], Peng Cui[a], Meicheng Li[a,*]

[a] State Key Laboratory of Alternate Electrical Power System with Renewable Energy Sources, School of Renewable Energy, North China Electric Power University, Beijing 102206, China

[b] Electronic & Magnetic Materials Department, Advanced Materials Division, Central Metallurgical Research and Development Institute (CMRDI), Helwan, P.O.Box 87, Cairo 11421, Egypt

ARTICLE INFO

Keywords:
Nickel Oxide
Low-cost
High-stability
Efficiency
Perovskite solar cells

ABSTRACT

Although revolutionary progress in power conversion efficiencies (PCEs) of perovskite solar cells (PSCs) greater than 22% has accompanied significant advances in materials engineering, processing, and device architectures, the selection of proper hole transporting materials (HTMs) is still critical for high efficiency, low-cost and long-term stability. The PSCs community is actively investigating a group of HTMs for high efficiency and long-term stability with commercial viability. In this context, inorganic nickel oxide (NiO_x)-HTMs possess the advantages of energetically favorable energy band positions, high hole mobility, superior chemical stability, and low cost manufacturing. Herein, we address the initial breakthroughs and recent progress in NiO_x-HTMs for PSCs. In addition to synthetic routes and deposition techniques used for NiO_x-HTMs in two major device architectures (p-i-n and n-i-p structure), the stability and cost-breakdown of PSCs are evaluated in details. Finally, future directions for further improvements on issues such as high efficiency, stability and low-cost of PSCs based on NiO_x-HTMs are also provided.

1. Introduction

The impressive development in the power conversion efficiency (PCE) of the organometal halide perovskite solar cells (PSCs) has charmed the photovoltaic community and attracted research attention due to the strong broadband absorption, tunable bandgap, high charge carrier mobility, long charge diffusion length, and low-cost fabrication of photo-active perovskite material [1–6]. The facile solution processability and ambipolar semiconducting features of the perovskite material further enable the fabrication of PSCs in variable device architectures [7]. Mihasaka and colleagues reported the first device based on CH_3NH_3PbBr with a PCE of 2.2%. In 2009, they were able to achieve 3.8% efficiency by substituting bromine with iodine, and use of iodide/triiodide redox electrolyte as a hole transporting medium in a dye-sensitized like structure and this was the time when the perovskite came to play a role in the energy conversion devices [8]. Later, Park et al. reported 6.5% PCE but with miserable stability owing to the used liquid electrolyte [9]. This has then lead to the first solid state device with a PCE of 9.7% employed scaffold mesoporous TiO_2 as electron transporting layer and 2,2′,7,7′-tetrakis(N,N-di-p-methoxyphenylamine)9,9′-spirobifluorene (spiro-OMeTAD) as hole transporting layer [10]. Since then, extensive efforts have been made in the modification of perovskite crystal/film composition and morphology [11,12], modification of the device architectures [13–15], and interfacial engineering [16–24]. Recently, several groups have been reported devices with PCE values of over 20% [11,25–29].

However, the state-of-the-art PSCs mostly require organic hole transporting materials (HTMs) such as poly-bis(4-phenyl)(2,4,6-trimethylphenyl)amine (PTAA), 2,2′,7,7′-tetrakis(N,N-di-p-methoxyphenyl-amine)9,9′-spirobifluorene (spiro-OMeTAD), poly(3,4-ethylenedioxythiophene) polystyrene sulfonate (PEDOT:PSS), and poly(3-hexylthiophene-2,5-diyl) (P3HT) [30–47]. These organic HTMs possess several drawbacks, such as tedious synthesis processes, poor crystallinity, low mobility, high cost, and possible degradation in moisture and air [44–51]. The choice of an ideal selective contact for sure will improve the charge dynamics to a great extent without introducing a degradation or deterioration of the perovskite absorbing layer and of great importance in scaling up the PSCs to the commercial application [20,50–54]. On the electron selective side, a handful variety of materials are made available to reduce the degradation and retard the

* Corresponding author.
E-mail address: mcli@ncepu.edu.cn (M. Li).

https://doi.org/10.1016/j.nanoen.2018.06.082
Received 21 May 2018; Received in revised form 11 June 2018; Accepted 25 June 2018
Available online 28 June 2018

charge carrier recombination. However, the portfolio becomes strictly limited when it comes to the hole transporting layers. Here, especially alternatives are very few when it comes to the inorganic counterparts which fulfill the thermal/chemical compatibility at the low processing temperature and high stability.

In the pursuit of stable and low-cost PSCs, devices with inorganic HTMs such as CuSCN, Cu_2O or CuO, $CuZnSnS_2$, WoO_3, $CuInS_2$ and NiO appear to be more promising [55–57]. In this context, the earth abundant NiO_x-HTMs have widely been used as a hole transporter in PSCs to replace the above mentioned organic HTMs with better stability and minimized charge losses [2,58–60]. The NiO_x can be a suitable candidate due to its p-type characteristics with a wide band gap (E_g > 3.50 eV), high optical transmittance, sufficient conductivity, chemical stability and an energetically favorable energy level alignment with various photoactive absorbers [61–63]. In addition, the NiO_x-HTMs can be processed easily *via* solution from corresponding precursors at low temperatures. Apart from these benefits, the choice of NiO_x-HTM in PSCs has also shown 90% stable performance for over 60 days of storage in air [13].

Inspired from the key role that the low-cost NiO-HTM plays in improving the PSC performance as well as in the stability of devices, this review will cover major advances of NiO_x-HTMs in PSCs that have been contributed to the recent efficiency and stability, including the evolution of device architectures, the development of the hole-selective layer deposition, synthesis, low-cost, morphology modification, and the interfacial engineering at perovskite/HTMs junction. The optimization of each layer with maintaining their charge mobility, electron balance and optical transmittance becomes typically necessary steps in the fabrication of both planar and mesoscopic p-i-n and n-i-p device architectures of PSCs. Finally, the challenges and future outlooks on further improvements on important issues such as high efficiency, stability and low-cost of PSCs incorporating NiO_x-HTMs will also be discussed.

2. Synthesis and fabrication route

2.1. Synthesis of NiO-nanopowder

The particle size and morphology are essential aspects to understand the macroscopic characteristics of materials, particularly for materials having morphological properties in nano-scale. At this stage, the ratio of surface area to volume and quantum size effect are greatly increased as compared to materials of larger grain sizes [64]. In this context, the synthesis and characterization of nanostructures play very important role in basic science and technological applications [65]. Among these nanoparticles, NiO nanoparticles are of technological importance due to wide range of applications as a p-type semiconductor with a stable wide bandgap energy (3.4–4.0 eV) [66].

NiO has octahedral Ni^{+2} and O^{-2} sites with rhombohedral or cubic crystal structure. The crystalline powder of NiO can be found as black or green with refractive index of 2.1818. The crystal and different powder, and corresponding X-ray diffraction of the NiO nanoparticles were shown in Fig. 1. The conductivity of NiO depends on the stoichiometric ratio. It has been revealed that stoichiometric NiO is insulating and p-type conductivity can be achieved by introducing nickel vacancies [67,68]. However, the large ionization energy associated with Ni vacancies deliver low hole density. In this regard, extrinsic dopants with more shallow acceptor levels are pleasurable to increase the hole mobility [68,69]. The extrinsic dopants such as Li, Cu, Mg, Cs and Co [70–73], as well as co-dopant like Li:Cu and Mg:Li [74–76] have been incorporated in NiO_x to enhance the charge carrier mobility and photon management. Recently, several groups have implemented the pristine or doped NiO_x-HTMs in PSCs with optimized efficiency over 20% which is comparable to that of PSCs based on organic-HTMs [7,70–77]. Therefore, the synthesis of NiO_x nanoparticles received considerable attention in this photovoltaic field.

This section will demonstrate the synthesis and characterization of NiO_x-nanostructures, starting from easily available materials (nickel chloride, nickel acetate, nickel nitrate, nickel hydroxide, nickel sulfate, and nickel formate *etc.)*. There is no doubt that the chemical solution routes in the synthesis of NiO_x-HTMs will pave the way for large-scale commercial deployment of the PSCs technology at low-cost.

2.1.1. Thermal decomposition

The synthesis of nanoparticles provides the various particle size alterations in terms of energy levels which can be tuned to match with perovskite materials, thereby enhancing the PCE. Generally, nanoparticles (quantum dot, quantum wire, quantum well, nanosheets *etc.)* have different characteristics than the bulk materials. Especially, hot carriers relaxation time and multiple exciton generation properties are helpful to increase the efficiency due to absorption of photon in different band gaps [78]. In this context, Dharmaraj et al. reported the synthesis of cubic NiO_x nanoparticles using a mixture of nickel acetate and poly (vinyl acetate) as precursor. The TEM images demonstrated that NiO_x nanoparticles have uniform size from 40 nm to 50 nm and well dispersed [79]. Since, 2D nano-structures have versatile applications due to their large surface area. Therefore, Zhang et al. documented a simple and convenient method to realize 2D-NiO_x nano-walls by thermal treatment of sputtered-Ni thin films [80]. These synthetic routes offer the large-scale production with low cost module construction and ease of synthesis. In addition, Gandhi et al. reported NiO_x nanoparticles with sizes of 3.5–12.4 nm by thermal decomposition of nickel acetate at different temperatures in NaCl and Li_2CO_3 as alkali salts [81].

The systematic tuning of the hole transporting properties through metal doped NiO_x also deserved attention. Yue et al. reported various amount (0–20%) of copper doping by a co-mixture of cupric acetate monohydrate and nickel acetate tetrahydrate in anhydrous ethanol (0.1 M) [73]. The ultraviolet photoelectron spectra revealed the Fermi level and valence band (V_B) *vs* vacuum level of NiO_x as 4.59–5.43 eV, 5% Cu-doped NiO_x as 4.58–5.51 eV and 20% Cu-doped NiO_x as 4.56–5.37 eV (Fig. 2a). This downward shift was helpful to V_B matching between Cu-doped NiO_x and perovskite absorber. In particular 5% Cu doping was efficient in collecting the photo-generated holes with less energy loss. On the other hand, high concentration of Cu in NiO_x displayed the upper shift of V_B position which further increased the energy loss for interfacial hole transport [82]. Plainly, the large quantity of extrinsic dopant would increase the defect density and interfacial trap-states in the NiO_x thin films, and thus decrease the photovoltaic performance, particularly V_{oc}, FF and charge carrier mobility. Furthermore, Chen et al. demonstrated the substitution of Ni atom in the stoichiometric ratio of NiO_x by Cs dopant [83]. The lattice distortion resulted in more amorphous phase in Cs:NiO_x compared to NiO_x due to the larger atomic radius of Cs (298 pm) than Ni (149 pm), this increases the Ni^{+3} acceptor ratio, and as a result the high hole conductivity [84,85]. The synthesis of Cs-doped NiO_x was done *via* cesium acetate with molar ratios of 0.5–3% mixed with $Ni(Ac)_2{\cdot}4H_2O$ solution. The best performance of Cs:NiO_x was attributed to 1% Cs doping. Additionally, a lower work function further highlighted the effective hole extraction as shown in Fig. 2b. Among the synthetic methods of NiO_x nanostructures, thermal decomposition route has been usually adopted due to the low temperature and no requirement of expensive apparatus.

2.1.2. Sono-chemical and sol-gel

Mourtada A. and co-worker reported a new technique for the fabrication of NiO_x. The Ni(II) Schiff base complexes have been synthesized using sono-chemical methods. Then, the nickel oxide nanopowder was obtained from the metal complexes after calcination at 650 °C for 2 h. The microstructure of the NiO_x powder appeared as cubic-like structure within particle size of 25 nm with direct band gap energy (E_g) of 2.37–3.6 eV [86]. The applications of sono-chemical routes led to a better mixing and deagglomeration of low-dimensional nanoparticles in corresponding precursors. This will further help to get smooth and

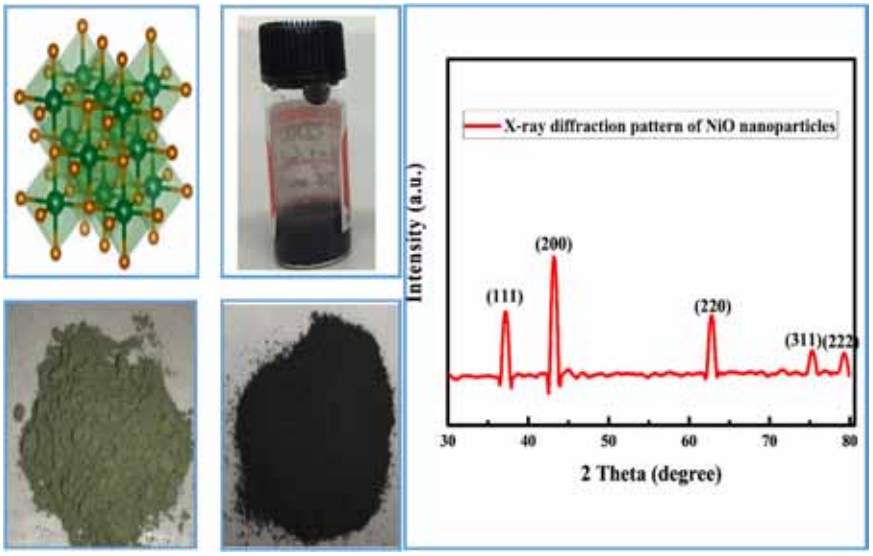

Fig. 1. Crystal structure, precursor solution, nanopowder and XRD pattern of NiO_x nanoparticles.

crack-free morphologies of hole transporting layers with less defect states. The synthesis of the NiO_x nanocrystals through sol-gel are typically prepared by dissolving nickel(II) acetylacetonate in diethanolamine, where the precursor needs heating up to 150 °C to form the sol suspension, which can be spin coated on the substrates. Moreover, the synthesis of NiO_x nanoparticles (19 nm) *via* alumina supported sol-gel process, citric acid as a ligand and $NiCl_2{\cdot}6H_2O$ precursors have also been reported [87]. In another study, Teoh et al. prepared NiO_x nanoparticles by sol-gel method which was accomplished by using poly (alkylene oxide) block copolymer as the surfactant and $Ni(NO_3)_2{\cdot}6H_2O$ as the inorganic precursor [88]. However, the crystallization of NiO_x needs high annealing temperature (500 °C) in sol-gel-processes as observed by Zhu et al. [89]. Although the adaptation of these processes are important in terms of thin films coating, special porosity and large area fabrication, the requirement of high annealing temperature limits their applications in flexible substrates.

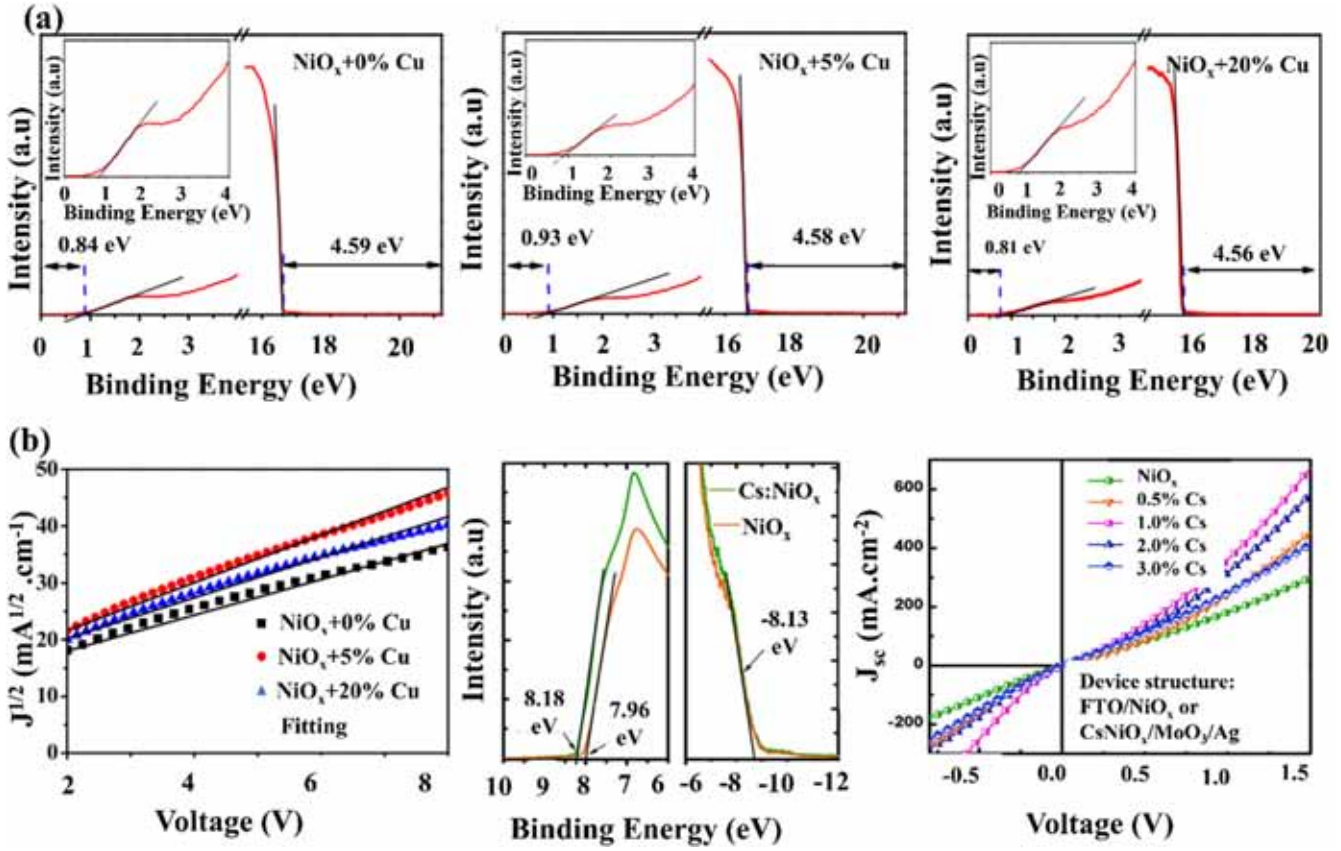

Fig. 2. (a) The ultraviolet photoelectron spectra of $Cu:NiO_x$ with $J^{1/2}$-V curves of the hole-only devices. (b) The UPS spectra, J-V curves of pristine NiO_x and $Cs:NiO_x$. Reprinted with permission from references [70,81].

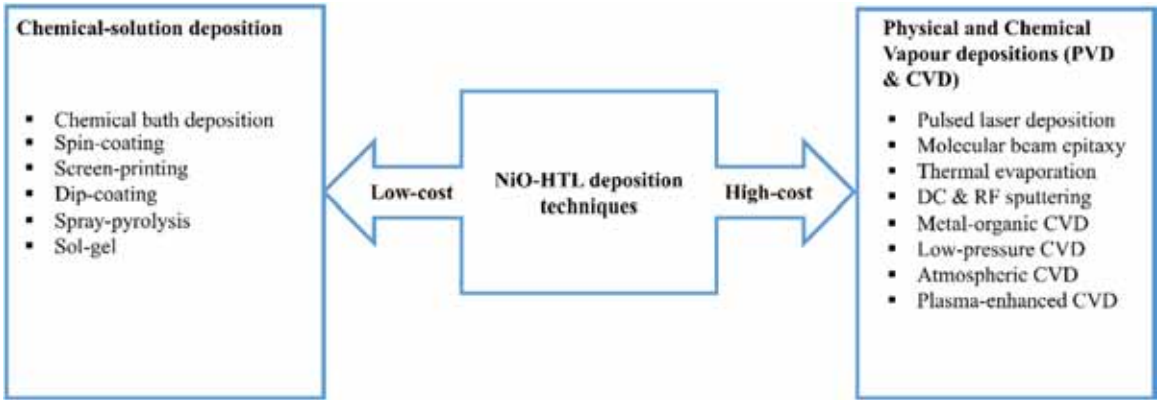

Fig. 3. Classification of fabrication techniques for NiO_x-HTL.

2.1.3. Chemical-combustion

Combustion chemistry is one of the viable routes to fabricate solution processable transition metal oxides (TMO) thin films with high crystallinity at low-temperature [90,91]. The sufficient energy generation and exothermic reaction occurring in combustion-processes will impart a lower transition energy, and thus a lower thermal energy for the shaping of TMO lattices. In contrast, the endothermic sol-gel reactions need significant external thermal energy to form TMO lattices and remove organic contaminant [92]. The combustion-processes have great potential in terms of low-temperature annealing of HTMs as illustrated in the following reactions [93].

(i) Conventional sol-gel route

$$Ni(CH_3OCO)_2.4H_2O + Cu(CH_3OCO)_2.H_2O \xrightarrow{>400^{\circ}C} Cu: NiO_{x(solid)} + 11H_2O_{(gas)} + 4CO_{2(gas)}$$

(ii) Chemical combustion route

$$Ni(NO_3)_2.6H_2O + Cu(NO_3)_2.3H_2O + CH_3COCH_2COCH_3 \xrightarrow{\sim 150^{\circ}C} Cu: NiO_{x(solid)} + H_2O_{(gas)} + N_{2(gas)} + CO_{2(gas)}$$

The Cu-doped NiO_x *via* chemical combustion of $Ni(NO_3)_2{\cdot}6H_2O$ (276.3 mg) and of Cu $(NO_3)_2{\cdot}3H_2O$ (12.1 mg) in 2-methoxyethanol (10 ml) with the addition of 10 μL of acetylacetone has been prepared by Jung et al. [94]. The solution-processed Cu:NiO_x revealed homogeneous morphology and high crystallinity at low temperature (150 ℃).

2.1.4. Chemical precipitation

The composite of NiO_x with multi-wall nano tubes have been prepared by Xiao-Ning Liao et al. through chemical precipitation with the addition of sodium dodecyl sulfate [95]. The $Ni(OH)_2$ precursors were prepared through the transformation of precipitation method, synthesized from $Na_2C_2O_4{\cdot}6H_2O$ and urea. And then, NiO_x samples have also been obtained by calcination $Ni(OH)_2$-precursor with different calcinations methods [96]. Furthermore, the diameter of crystalline NiO_x in nanoscale of ~ 2 nm has been reported by thermal decomposition of nickel sulfate using homogeneous precipitation. Similarly, NiO_x-nanostructure has been derived from a homogeneous precipitation method with an aqueous solution of nickel nitrate hexahydrate and urea [97]. The chemical reaction has been demonstrated by using $NiCl_2$ and NaOH as starting materials. Next, nickel hydroxide precursor was formed by dehydration and resulted in NiO_x nanocrystals with rod like morphology. In addition, through chemical synthetic route, defect free NiO_x nanoparticles with diameter ~ 40 nm shown great interest as well [98]. Moreover, Ghosh et al. prepared NiO_x nanoparticles by the oxidation of Ni nanoparticles [99]. Interestingly, NiO_x nanoparticles have been prepared by a simple aqueous solution of materials containing Ni source with urea as precipitant. Chandrappa et al. documented a size series of ligand-stabilized Ni nanoparticles by solution chemistry with diameter of 8–24 nm. Then, Ni(core)/NiO_x (shell) with thickness of 2–3 nm have been formed by solution-phase oxidation in atmospheric oxygen at 200 ℃ [100]. Additionally, $Ni(NO_3)_2{\cdot}6H_2O$ (oxidizer) and sugar (dextrose as fuel) could be another route to prepare nanocrystalline NiO_x. These methods consider as simple, fast, economical and eco-friendly. Collectively, the simple solution methods would be the promising techniques in order to prepare low-cost NiO_x-nanostructures and fabricate as HTLs in the field of low-cost and stable PSCs.

2.2. Fabrication of NiO_x hole transporting layers

Thin film deposition of NiO as HTL can be categorized into physical or chemical processes. The chemical fabrication consist of gas-phase and solution depositions. Additionally, the gas-phase methods include: chemical vapour deposition (CVD), atomic layer epitaxy, and atomic layer deposition (ALD) [101,102], while solution-depositions attribute to spray pyrolysis, sol-gel, spin, and dip-coating [73,94,103–105]. On the other hand, physical processes composed of pulsed laser deposition (PLD) [106], physical vapour deposition (PVD) [107], molecular beam epitaxy [108], and magnetron sputtering [109]. In addition, other techniques such as chemical bath deposition, advanced reactive gas deposition, electron beam evaporation, vacuum evaporation, anodic oxidation, radio frequency sputtering, electron beam evaporation, DC-magnetron sputtering, anodic/cathodic electrodeposition have also been performed for NiO_x-thin films deposition [110–115]. Plainly, we classify the above mentioned techniques in Fig. 3. Herein, we will focus on pristine and doped NiO_x thin films fabrications with respect to the cost of techniques and the best performance of obtained PSCs.

2.2.1. Physical and chemical vapour deposition techniques

Here we will discuss the enhanced quality and homogeneity of NiO_x thin layers prepared by sputtering, pulsed laser deposition (PLD) and atomic layer deposition (ALD). NiO has a stable ionic cubic crystal structure (space group of $Fm\bar{3}m$) with a melting point of 1955 ℃. The high bonding strength holds ions firm, which make NiO layer intrinsically insulator if the thickness increases than a few nanometers [116]. Most of the deposition techniques reported the best photovoltaic parameters with the lowest NiO-HTL thicknesses of 7–20 nm, due to the limitation of uniform film coverage [117–119]. If NiO-HTLs are deposited as ultrathin, where the film thickness is comparable to the characteristic length of the space charge region (Debye length) and which have high conformality, the films will have a higher electrical conductivity without sacrificing optical transparency. Different conductivity behaviors of NiO-HTL are expected when the film thickness is comparable to or smaller than the width of the Debye length (L_D) as described by Eq. (1), which depends on the material preparation,

dielectric constant, and carrier concentration of the material. At this stage, NiO loses its bulk properties and produces anomalous transport properties.

$$L_D = \sqrt{\varepsilon_0 \varepsilon_r k/Tq^2N} \quad (1)$$

where ε_0 is the permittivity of free space, ε_r is the relative dielectric constant of the material, k is the Boltzmann constant, T is the temperature, N is the carrier concentration, and q is unit charge. Additionally, NiO has defective surface hydroxyl group (NiOOH) with a deeper valence band level than NiO, which consequently limits the hole transport from perovskite to NiO. Thus, a greatly improved performance of NiO as HTL in PSCs through the control of not only its thickness but also surface hydroxyl groups have been investigated by many researchers [120–122]. In this regard, Ahmadi et al. demonstrated a modified DC reactive magnetron sputtering technique for the deposition of NiO_x/Ni bilayer as HTL/back-contact coupled in normal architecture (n-i-p) of PSCs at low-temperature. Here, the low-temperature sputtering of NiO_x-HTL resulted in uniform and crack-free coverage of perovskite layer. The PSCs showed stability up to 60 days due to the protection of perovskite by NiO_x/Ni bilayer [57]. Similarly, Chen et al. reported the low-temperature sputtering for NiO_x-HTL in the inverted structure of PSCs with mesoporous-NiO_x layer (200–250 nm)/ sputtered-NiO_x layer (9.5–10.5 nm). The PSCs achieved by this technique delivered a V_{oc} of 0.95 V, J_{sc} of 19.8 mA cm^{-2}, FF of 61% and PCE of 11.6% [123]. Similarly, NiO_x-HTM and conductive electrode obtained from Ni/Au bilayer through oxidizing the e-beam-sputtered film in O_2 atmosphere. The bi-functional p-type electrode of Ni (10 nm) and Au (7 nm) showed high transparency, great electrical conductivity and favorable work function matching with the valence band position of perovskite which are the desirable factors to obtain high performance of PSCs [124]. Subbiah et al. further used electrodeposited NiO_x-HTLs in p-i-n device structure [125], and demonstrated superior performance due to decreased series resistance and high shunt resistance [126]. Though, magnetron sputtering is the most promising technique for making NiO_x-thin films at large-scale industrial lines, the issues of small FF and low J_{sc} are still need to be addressed. In this context, dopants such as Li, Cu and Mg fractions in NiO_x have been reported by co-sputtering process to improve FF and J_{sc} [127]. There is no doubt that the increasing nickel vacancy, namely Ni^{+3} acceptor, is an effective way to render NiO more conductive. Therefore, the high conductivity of metal-doped NiO_x originates from the increased Ni^{+3} acceptors. The doping of NiO_x with Mg, Li or Cu will enhance the conductivity, but these dopants will create an absorption loss [128,129]. In this context, PLD and ALD have been performed to enhance the quality and homogeneity of NiO_x thin layers in high-efficiency NiO_x-HTM-based PSCs. Particularly, Park et al. performed PLD to optimize NiO_x thin film. The best PSCs based on 150 nm thin layers of NiO_x delivered PCEs of 17.3%, J_{sc} of 20.2 mA cm^{-2}, V_{oc} of 1.06 V and FF of 81.3% [130]. Further, Seo et al. fabricated an ultra-thin film of un-doped NiO_x films with less absorption loss by ALD without any pinholes, and achieved higher J_{sc} and FF values [121]. Furthermore, several reports have also investigated the effect of NiO-hole selective layer thickness on the PSCs performance [56,131–134]. A very thin film creates a serious short circuit due to the large amount of pinholes and leakage paths, which fails to selectively collect holes and block electrons efficiently. A thick NiO_x film, on the other hand, absorbs much incident light but contributes little to photocurrent, reducing J_{sc}. This also suggests that thick NiO_x film would increase series resistance and prevent effective holes collection, causing a loss in photocurrent and deteriorated FF. The photovoltaic parameters as a function of NiO_x-HTL thickness are shown in Fig. 4 and Table 1. Although, ALD and PLD are the potential choices to increase the conversion efficiency of PSCs based on NiO through maximizing the properties and thin film quality, the high cost of equipment and controlled conditions are the remaining issues to be addressed for the commercial viability of these technologies.

2.2.2. Chemical-solution deposition techniques

To realize low-cost deposition processes for high-performance NiO_x-HTLs, it has recently become important to understand the properties and structures of solution-processed NiO_x nanoparticles or nanocrystals films. Specifically, to select a suitable process to produce NiO_x-HTLs to meet the demands of a realistic situation, it is necessary to know the critical differences in film density, morphology, and transition temperature. The solution-processed techniques such as spin-coating and screen-printing are mostly reported for NiO_x films. However, the differences between the films fabricated by these processes are not yet sufficiently clear. Yin et al. employed solvothermal method and achieved NiO_x nanoparticles ~ 3- nm. The colloidal precursor has been prepared by dispersing the NiO_x nanopowder into ethanol with certain amount of acetic acid as a stabilizer. Then, the obtained precursor was coated on conducting glass with an annealing temperature of 300 ℃ to remove residual acetic acid (Fig. 5a) [136]. Hu et al. obtained the NiO_x precursor from nickel acetate tetrahydrate mixed in monoethanolamine and methoxyethanol. This method supported a high quality of $CH_3NH_3PbI_3$ on the surface of 10 nm spin-coated NiO_x-film as shown in Fig. 5b [132]. It is worth notable that well-connected film of NiO_x nanocrystals (10–40 nm) has the ability to extract hole efficiently from the perovskite layer with less energy loss [56]. Additionally, the nucleation growth of perovskite over NiO_x-films can further improve the photovoltaic performance of PSCs as well. In this regard, You et al. facilitated the effective nucleation sites for the growth of perovskite crystals on spin-coated (80 nm) thin film of NiO_x. The as prepared NiO_x layer provided better crystallinity of the perovskite film which further helped in more photon harvesting [137].

Based on solvent engineering approach, Hou et al. deposited a dense and uniform perovskite layer with grain size 300–500 nm on the top of low-temperature NiO_x spin-coated substrate. The method has been summarized with dry NiO_x nanopowder prepared by flame spray technique from nickel acetate in 2-ethylhexanoic acid, xylene and ignited by a premixed methane-oxygen flame to get compact and well-connected morphology (Fig. 5c) [138]. Moreover, Liu et al. synthesized flower like NiO_x nanosheets from nickel(II)nitrate hexahydrate dissolved in deionized water. The aqueous solution of oxalic acid dehydrate and hexamethylenetetramine were added drop wise under stirring. The porous NiO_x nanosheets paste prepared by mixing ethyl cellulose, ethanol, terpineol and NiO_x nanosheets powder. The as screen-printed NiO_x (NSs) film provided larger pore size and facilitated the infiltration of perovskite with reduced charge recombination [139]. Additionally, Guo et al. fabricated 2D-nanosheets of NiO_x *via* dissolving nickelous acetate tetrahydrate with urea, ethanol and distil water [140].

Similarly, Cao et al. also demonstrated a mesoscopic PSCs with quadruple-layer consisted of inorganic metal oxides combine with carbon counter electrode. Here, screen-printed NiO_x HTL has been synthesized from NiO_x nanopowder mixed with ethyl cellulose solution in ethanol and terpineol [141]. In total, the diffusion of perovskite material were facilitated with large amount of excitons in mesoporous structures. The application of pristine NiO_x was also tested in high performance of flexible and rigid PSCs with spin-coated NiO_x-HTLs (20 nm) from 2 wt% of NiO_x ink at controllable room-temperature (without post-annealing) as shown in Fig. 5d [122]. In addition, Kim et al. used a solution-processed copper-doped NiO_x (Cu:NiO_x) as HTM in order to obtain high-performance and environmentally stable PSCs. Furthermore, the PCE based on sol-gel-processed Cu:NiO_x-HTMs has been improved from 9% to 15.4%, demonstrating the potential applications of Cu:NiO_x in efficient PSCs [142]. However, the sol-gel-derived Cu:NiO_x-HTM needs high annealing temperature (> 400 ℃) to get high crystallinity. The high-temperature treatment not only will increase the cost of PSCs but also originate the incompatibility with polymer substrates for roll-to-roll fabrication. Regarding these shortcomings, Jung et al. fabricated combustion-processed Cu:NiO_x thin film of 50 nm at 150 ℃ with high crystallinity and transmittance accompanied by

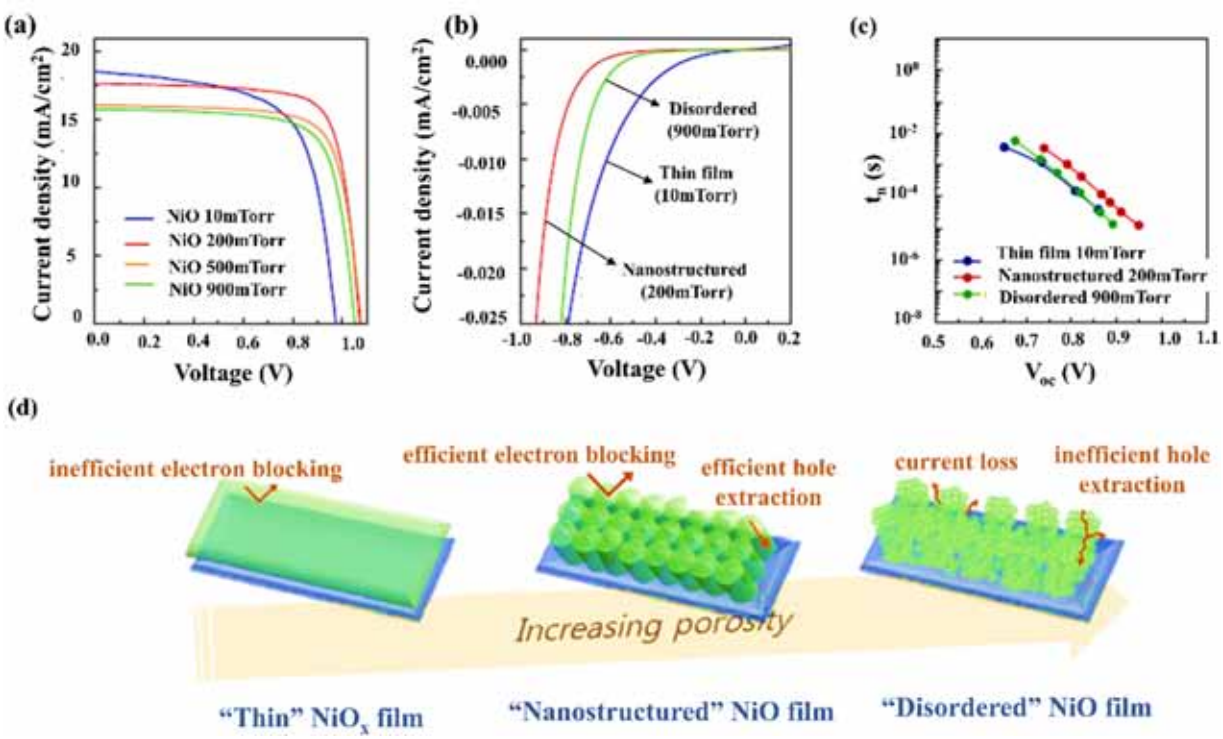

Fig. 4. Morphological effect and growth of the PLD-NiO-HTL. (a) The J-V characteristic curves of PSCs based on PLD-NiO films with different thicknesses. (b) J-V at dark. (c) The recombination lifetime of the devices. (d) Schematic illustration of thin, nanostructured, and disordered NiO-layers. Reprinted with permission from reference [127].

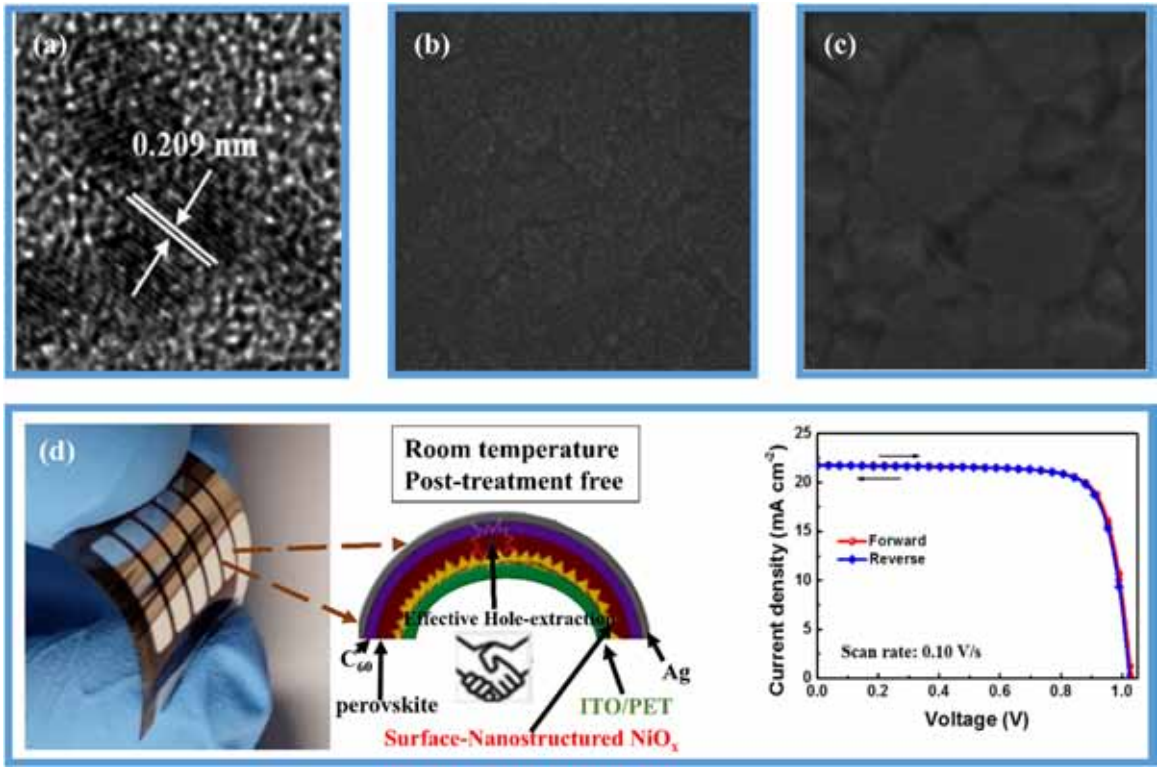

Fig. 5. (a-c) SEM images of NiO_x-HTLs with different deposition approaches. (d) Post-annealing free deposition of NiO_x-HTLs in flexible PSCs. Reprinted with permission from references [120,128,129,131].

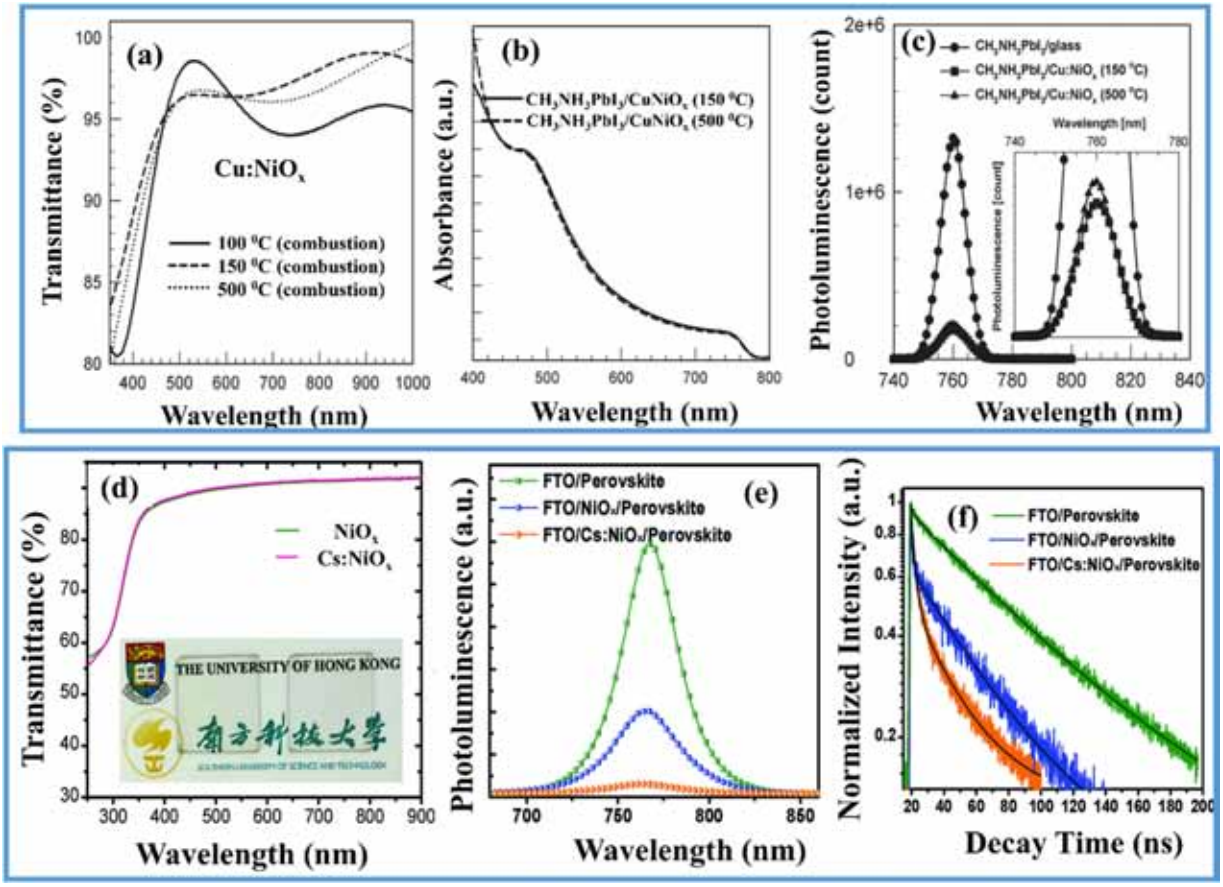

Fig. 6. (a-c) Transmittance spectra, UV–vis absorption spectra, and steady-state PL of Cu:NiO_x films fabricated *via* combustion and conventional sol-gel routes. (d-f) Transmittance spectra, PL and time resolved PL spectra for NiO_x/perovskite and Cs:NiO_x/perovskite. Reprinted with permission from references [81,92].

smooth and compact surface morphology [94]. Additionally, the broad light-absorption of Cu:NiO_x in the long wavelength region was attributed to the different degree of Ni vacancies (Fig. 6a). This region was suitable to absorb more incident photon by the incorporation of $CH_3NH_3PbI_3$ light absorber (Fig. 6b). The four-point probe measurement revealed higher electrical conductivity from 7.54×10^{-4} S cm^{-1} to 1.25×10^{-3} S cm^{-1} which was further confirmed by steady-state PL quenching (Fig. 6c). Moreover, Chen et al. prepared Cs doped-NiO_x films with 90% transmittance in the range of 400–800 nm as illustrated in Fig. 6d [83]. The high transparency of HTLs is pleasurable for minimize optical losses and thus for photovoltaic devices to harvest more photon. The smooth surface morphology and full coverage formation of perovskite were resulted in enhanced photovoltaic parameters as confirmed by PL and time-resolved PL spectra depicted in Fig. 6e, f.

Recently, the investigation on the influence of Cu doping with different concentration in NiO_x film has been demonstrated by Yue et al. [73]. The incorporation of 5% Cu in NiO_x revealed the highest mobility of hole. This trend of hole mobility was described by the following Eq. (2):

$$J_D = \frac{9\mu\varepsilon\varepsilon.V^2}{8L^2}, \tag{2}$$

where J_D, μ, ε, ε_0, V and L represent the dark current, hole mobility, relative dielectric constant of active material, vacuum permittivity, applied voltage and thickness of absorber layer, respectively. The larger slope of the $J^{1/2}$ *vs.* V curve was associated with higher value of hole mobility as shown in Fig. 2a. The improvement in optimized PCE of 20.5% was mainly attributed to the lower density of hole-trapping states. There is no doubt that the solution based chemistry for thin films deposition provide high purity products at low-cost, starting from easily available materials. In particular, spin-coating and screen-printing techniques are beneficial for varieties of uniform thin films on a large area of PSCs. However, the optimization of preparative conditions is the main requirement for obtaining high quality NiO_x-films. In addition, the NiO_x-HTLs have the prominent problems of low FF and V_{oc} in particular when fabricated by solution processes compared to organic HTLs [121]. It is concluded that an ideal p-NiO_x films should have high optical transparency, high electrical conductivity, decent charge transporting/blocking capability, low-sintering temperature and suitable interfacial energy for perovskite crystals growth.

3. Architectures of PSCs based on NiO_x-HTMs

There are two major device architectures (planar/mesoporous p-i-n and n-i-p structure) of PSCs, which are composed of photoactive perovskite layer, charge transporting and collecting layers (HTLs, ETLs and corresponding electrodes) as schematically shown in Fig. 7. In addition, we also comment that the kinetic processes and influencing factors have significant roles in light and charge carrier management. The influencing factors that affect the function of HTLs/ETLs are very important to understand the underlying causes of photovoltaic performance. This section will describe these factors associated with NiO_x-HTLs which will further overview with recent developments and efforts related and their corresponding optimizations. The influencing factors are schematically shown in Fig. 7 and summarized as:

i. Energy band alignment (influence charge injection and recombination)
ii. Charge carrier management (influence photo-generated charge and

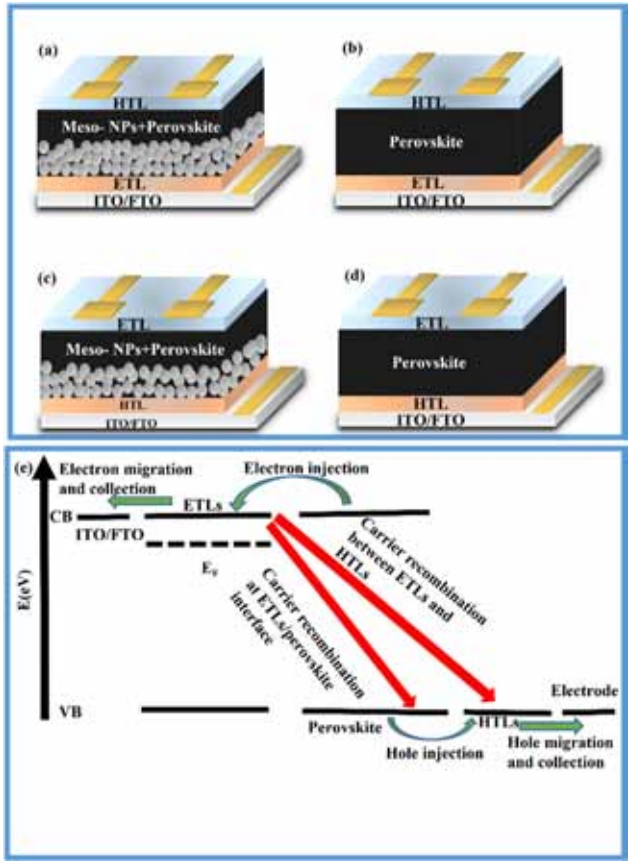

Fig. 7. Schematic illustration of perovskite solar cell (PSC) architectures. (a, b) Mesoporous and planar n-i-p PSCs. (c, d) Mesoporous and planar p-i-n PSCs. (e) Working mechanism in PSC.

collection)

iii. Trap states (influence charge transport and recombination)
iv. Electrical conductivity (influence charge transport and collection)
v. Interface (influence charge recombination)
vi. Morphology (influence the contact with perovskite and its deposition)

Initially, the incorporation of NiO_x-HTMs was aimed to obtain a greater solar spectrum and higher V_{oc} by making a tandem structure combined with an n-type TiO_2-based photo-anode [143,144]. Further, Irwin et al. successfully demonstrated the first replacement of unstable PEDOT:PSS by NiO_x in organic photovoltaic (OPV) with enhanced stability and reduced hysteresis [137,145]. Lately, Steirer et al. developed a relatively simple solution-processed NiO_x-thin interlayer on glass/ITO electrode. It was demonstrated that NiO_x has efficient hole conductivity and tunable work function ranged from 5.0 to 5.6 eV. In addition, its inertness without corrosion to ITO/FTO substrates and deeper work function were pleasurable to enhance stability and V_{oc} of PSCs [132,146].

The planar PSCs-based on NiO_x-HTMs have unique features due to its relatively low-temperature solution processing compared to the mesoporous PSCs that need high-temperature sintering (> 450 °C). However, planar PSCs geometry suffers from a smaller interfacial area between the light absorber and the HTLs/ETLs. Therefore, the selection of suitable charge transporting layers is urgent for improving photovoltaic performance. In this regard, solution-processed inorganic NiO_x-HTLs counterparts with high transparency and appropriate work function are promising alternatives for high-performance PSCs. The NiO_x-HTLs offer great promises as hole selective contact in PSCs due to its high conductivity, high optical transmittance, and deep-lying valence band (V_B) that matches well with the V_B of methylammonium lead halide. In contrast, the other organic-HTMs that require tedious multi-step organic synthesis and purification, NiO_x can be prepared by simple and low-cost synthetic processes. The first reported article on planar structure of $NiO_x/CH_3NH_3PbI_{3-x}Cl_x$/PCBM documented a low efficiency (< 0.1%) mainly due to very poor perovskite coverage on the NiO_x surface [147]. Since then, many efforts have been devoted to improve the device efficiency over 20% using pristine or doped NiO_x as HTLs [73,77]. The details will be discussed in the following device configurations.

3.1. Mesoporous (n-i-p) perovskite solar cells

Burschka et al. employed NiO_x nanoparticles to form a mesoporous NiO_x space separator between mesoporous TiO_2 and carbon counter electrode in the device configuration of FTO/compact-TiO_2/meso-TiO_2/meso-NiO_x/carbon. The hetero-p-n junction formed by NiO_x/TiO_2 interface facilitated the transport and extraction of holes/electrons in opposite directions [148,149]. In another report, Liu et al. applied highly crystalline NiO_x nanosheets with additional mesoporous ZrO_2 layer in n-i-p heterojunction. Here, the ZrO_2 layer worked as a separator for the meso-TiO_2 and meso-NiO_x layers to further suppress charge recombination at TiO_2/NiO_x interface. The device configuration of FTO/compact-TiO_2/meso-TiO_2/meso-ZrO_2/meso-NiO_x/carbon sequentially deposited with $CH_3NH_3PbI_3$ delivered a PCE of 14.2% with excellent stability [139]. Similarly, Xu et al. used a doctor-blade technique to fabricate mesoscopic $TiO_2/ZrO_2/NiO_x$/carbon structure with increased PCE of 14.9% [150]. Under similar configuration, a quadruple scaffold-layer composed of mesoscopic $TiO_2/Al_2O_3/NiO_x$/carbon was deposited by screen-printing with a PCE of 15.03% [141]. The above mentioned mesoscopic devices displayed high stability due to the protection provided by all-inorganic transporting layers and carbon counter electrode. However, it is critical to control the mesoscopic layer thickness which will further introduce the trap states, and thus low charge transport with high recombination rate. In this context, the wetting properties, perovskite morphology, absorption and hole extraction process with a suitable surface treatment of NiO_x-HTLs can significantly enhance the FF and J_{sc}.

3.2. Planar (n-i-p) perovskite solar cells

The NiO_x-HTMs have significant impacts on hole extraction and long term stability of PSCs. For instance, NiO_x-HTLs have been demonstrated in regular mesoporous carbon electrode based PSCs, however, it is very challenging to direct deposit NiO_x-HTMs on the top of perovskite layer in planar n-i-p devices because the solvents used for the dispersion of NiO_x-HTMs are mostly strong polar organic or water [151]. Therefore, it is very important to explore a general and facile approach to fabricate NiO_x-HTLs that possess thermal/chemical compatibility with perovskite materials. To improve the extraction of photo-generated holes, modified sputtering technique was introduced for the fabrication of NiO_x thin film on perovskite layer. Additionally, the sputtered-nickel electrode was deposited by keeping the vicinity of work function close to the V_B of perovskite layer to replace the expensive Au contact. This approach resulted in compact and uniform NiO_x layer coverage on perovskite layer. The periodic deposition by controlling the temperature, led to lower the substrate temperature, which helped to safe perovskite layer from damages. The obtained planar n-i-p PSC composed of FTO/compact-$TiO_2/CH_3NH_3PbI_{3-x}Cl_x/NiO_x$/Ni initially delivered low photovoltaic performance due to the strain introduced by sputtering process. However, after the strain released by cooling the sputtered-NiO_x layer, high hole mobility led to improve both V_{oc} and J_{sc}. Eventually, PCE of the obtained PSC has been increased up to 7.24% with impressive long-term durability over 60 days. The NiO_x-HTLs in planar n-i-p PSCs promise a new window which would effectively hinder the penetration of water and oxygen [57,152].

3.3. Mesoporous (p-i-n) perovskite solar cells

Tian et al. fabricated the mesoporous NiO_x-based PSCs with device configuration of FTO/compact-NiO_x/meso-NiO_x/$CH_3NH_3PbI_3$/PCBM/Al. After controlling the thickness of compact and mesoporous NiO_x films up to 80 nm and 120 nm respectively, the best device delivered a PCE of 1.5% with very low FF and J_{sc} due to high resistance at NiO_x/absorber interface [153]. Another group incorporated a mesoporous NiO_x as a host to adsorb more amount of perovskite for the improvement of photon harvesting. It was confirmed that the V_B alignment of NiO_x and conduction band (V_C) of $PC_{61}BM$ with perovskite were suitable for receiving high output voltage and minimizing the energy losses for the charge separation process between the active layer and selective contacts. The best device delivered V_{oc} of 1.04 V, J_{sc} of 13.24 mA cm^{-2}, FF of 69% and a PCE of 9.51% [60]. By elimination of compact NiO_x layer, Zhu et al. employed an extremely thin mesoporous NiO_x layer in FTO/meso-NiO_x/$CH_3NH_3PbI_3$/PCBM/Au structure to obtain efficient PSCs. Plainly, a corrugated surface from aggregation of facet NiO_x nanocrystals facilitated perovskite formation with better coverage and interconnectivity. The electron blocking ability to reduce the charge recombination and leakage current was attributed to 40 nm thick meso-NiO_x. The best performance of NiO_x-based PSCs displayed a V_{oc} of 0.882 V, J_{sc} of 16.27 mA cm^{-2}, FF of 63.5% and PCE of 9.11% [56]. Furthermore, another group introduced a low-temperature sputtered-NiO_x film to serve as pinhole-free compact layer for optimizing charge collection losses in NiO_x/perovskite interface. A high quality NiO_x-compact layer benefited the charge collection and improvement in the device reproducibility as compared to the PSCs employing solution-processed-NiO_x [60]. By optimizing the oxygen doping of 10% and the thickness of meso-NiO_x layer during sputtering process, a decent PCE of 11.6% has been demonstrated [123]. The long-life of holes in the mesoporous-NiO_x have been identified with improved charge separation at the NiO_x/absorber interface for efficient mesoporous NiO_x-based PSCs. However, it is very critical to reduce the meso-NiO_x thickness and optimize the interfacial contact of NiO_x with perovskite. In this regard, replacement of non-injected scaffold was suggested to minimize the interface recombination [154]. Chen et al. reported a hybrid interfacial layer by employing an ultra-thin compact NiO_x layer with thin mesoporous Al_2O_3 scaffold in inverted PSCs with FTO/compact-NiO_x/meso-Al_2O_3/$CH_3NH_3PbI_3$/PCBM/BCP/Ag configuration [119]. The hybrid interfacial layer significantly minimized the interfacial recombination losses. The compact-NiO_x layer and highly transparent meso-Al_2O_3 were helpful to prevent light absorption losses. Additionally, the possible shunt paths between FTO and absorber material were also inhibited by introducing Al_2O_3 nanoparticles on the pinholes of compact NiO_x layer.

3.4. Planar (p-i-n) perovskite solar cells

For the first time, planar PSCs have been reported with a solution-processed NiO_x thin films by Jeng et al. [62]. The NiO_x-HTL was positioned as an electrode interlayer on the ITO substrate to realize $CH_3NH_3PbI_3$/PCBM hybrid solar cells. One of the main problems with the stated planar devices was the pin-holes in the deposited NiO_x-HTLs. The UV-ozone treatment was performed to improve surface wetting capability. The work function of NiO_x thin film was also modified up to 5.4 eV to achieve alignment with the V_B of $CH_3NH_3PbI_3$. The hybrid cell composed of ITO/NiO_x/$CH_3NH_3PbI_3$/PCBM/BCP/Al delivered a PCE of 7.8%. Furthermore, Lai et al. proposed oxidized-Ni metal with an annealing temperature of 450 °C to realize the smooth surface morphology of NiO_x film and facilitated perovskite interconnectivity with pinhole-free surface coverage [155]. The same group further prepared Ni (10 nm)/Au (7 nm)-bilayer as HTM when oxidized by e-beam-sputtering in O_2 atmosphere with annealing temperature of 500 °C. This HTM delivered optical transparency > 60% in the visible spectrum, good electrical conductivity and favorable work function matching to the V_B of active layer. Transparent conductive oxides-free PSCs has been fabricated with device configuration of glass/Au:NiO_x/$CH_3NH_3PbI_3$/C_{60}/BCP/Al. This approach demonstrated a J_{sc} of 13.04 mA cm^{-2}, V_{oc} of 1.02 V, FF of 77% and PCE of 10.24%. The improvements of V_{oc} and FF occurred due to minimize energy loss and superior conductivity [124]. Later on, Subbiah et al. used electro-deposited-NiO_x and CuSCN films as HTMs in FTO/HTM/$CH_3NH_3PbI_{3-x}Cl_x$/PCBM/Al device. In comparison NiO_x-based PSCs delivered better performance than the CuSCN due to lower series resistance and higher shunt resistance. It has been mentioned that UVO treatment further improved the J_{sc} up to 14.2 mA cm^{-2}, V_{oc} to 0.786 V, FF to 65% and PCE to 7.26% [125]. Similarly, Hu et al. fabricated PSCs based on NiO_x compact layer with improved PCE of 7.6% [132]. Cui et al. employed the reactive magnetron sputtering to further improve the quality of NiO_x-compact films. Here the solvent-engineering method has been used to form a homogeneous surface coverage and uniform interlayer morphology of perovskite onto the compact-NiO_x HTLs. The as prepared device with a 240 nm thick absorber layer and NiO_x electrode presented a PCE of 9.84% [118].

Generally, the NiO_x-based PSCs exhibited higher V_{oc} and a lower FF compared to organic-HTMs devices. The higher V_{oc} is due to the V_B matching between NiO_x-HTM and perovskite while lower FF is caused by the poor interconnectivity at the interface of HTM and photoactive material [156]. Therefore, Park et al. used hybrid NiO_x/PEDOT-HTMs in PSCs to improve FF. The addition of PEDOT covered the NiO_x-coated substrate with a modified rough morphology. This approach improved the interface of NiO_x/perovskite heterojunction with reduce interfacial trap-states. The lower charge transfer resistance at the interface of NiO_x/perovskite demonstrated a hysteresis-free behavior with a PCE of 15.1% [157]. Park et al. further modified the NiO_x/perovskite interface through pulse laser deposition (PLD) to fabricate a well-ordered nanostructured-NiO_x thin film with high optical transparency and preferred orientation of (111) plane. This orientation of NiO_x showed a lower resistivity and reduce sheet resistance with efficient hole extraction compared to other growth direction [130]. The champion device displayed a J_{sc} of 20.2 mA cm^{-2}, V_{oc} of 1.06 V, FF of 81.3% with a remarkable efficiency of 17.3%. Further to simplify the deposition procedure, Yin et al. used solution-processed NiO_x film to fabricate an inverted planar PSCs [146]. It has been mentioned that the thickness of NiO_x film significantly influenced the photovoltaic performance, hysteresis effect and air storage stability of the as prepared devices. However, with a suitable thickness of 90 nm and nanostructure roughness of 3.835 nm of NiO_x layer, hysteresis-free devices were fabricated. Moreover, spin-coated NiO_x film was also applied to flexible PET substrate (PCE of 14.53%) and rigid substrate (PCE of 17.60%) by Zhang et al. [122]. The improved performance were attributed to efficient hole extraction, reduce interfacial and monomolecular Shockley-Read-Hall recombination in these architectures.

It is worth notable that most of the above mentioned structures containing PCBM as an ETL, which is an issue of cost and stability. Replacing organic charge extraction layers with inorganic materials would provide device durability, versatile choices for material selection, and device design with low-cost production. For the fabrication of stable and low-cost PSCs, You et al. reported planar PSCs (ITO/NiO_x/$CH_3NH_3PbI_3$/ZnO/Al) with all solution-processed metal oxide charge transporting layers [158]. The favorable band alignment between inorganic charge transporting layers accompanied by high crystallinity of perovskite film on NiO_x, led to enhance V_{oc} as compared to PSCs based on PEDOT:PSS-HTLs. The strong hole/electron blocking effects originating from the deep-valence band of ZnO/deep-conduction band of NiO_x resulted in a higher J_{sc} of 21.0 mA cm^{-2}, V_{oc} of 1.01 V, FF of 76%, and PCE of 16.1%. Additionally, the protection of perovskite material by NiO_x-HTMs and ZnO-ETLs resulted in high-stability of PSCs against water and oxygen degradation as shown in Fig. 8a. The stability improvement can also be attributed to the organic (C=C bond)-free and chemically stable inorganic charge transporters compared to organic

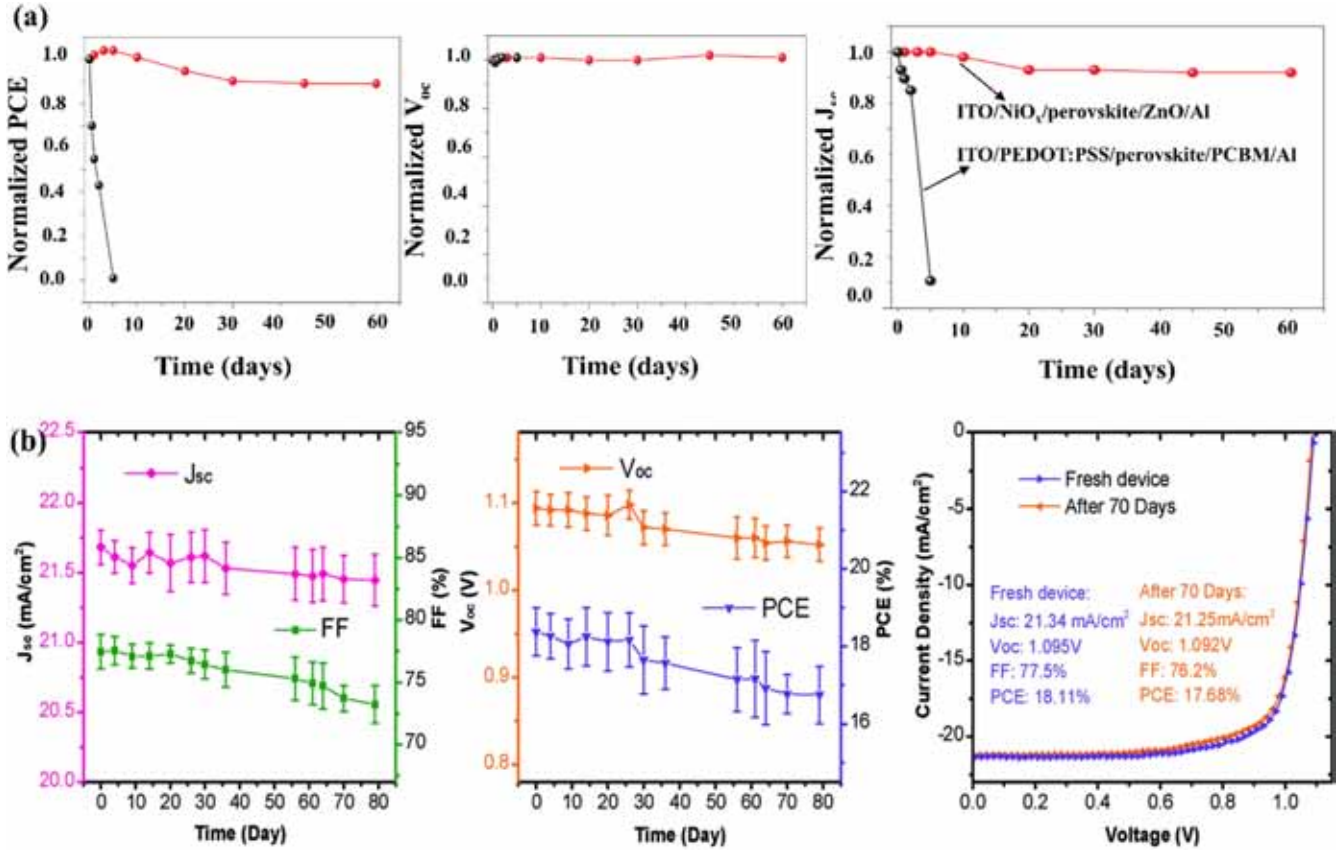

Fig. 8. (a) Stability of photovoltaic parameters of un-encapsulated PSCs based on PEDOT:PSS (black) and NiO_x-HTMs (red) at ambient condition. (b) Photovoltaic parameters and *J-V* characteristic curves of encapsulated Cs:NiO_x PSCs. Reprinted with permission from references [81,150].

charge transporting layers.

Later on, it was realized that doping of NiO_x-HTMs could be an effective way to improve the performance of the PSCs. In this context, Kim et al. employed the doping method in planar PSC *via* sol-gel processed copper (Cu)-doped NiO_x at 500 ℃ annealing temperature to achieve high crystallinity. The device structure of ITO/Cu:NiO_x/$CH_3NH_3PbI_3$/$PC_{61}BM$/C_{60}/Ag displayed a PCE of 15.4%. The improvement in photovoltaic parameters was attributed to the enhanced electrical conductivity, charge collection capability and favorable perovskite crystallinity on Cu:NiO_x film [142]. In addition, it has been also confirmed by the same group that the application of wider band gap of Br-doped perovskite absorber in Cu:NiO_x-based PSCs further increase the V_{oc} from 1.13 V to 1.16 V. In the same progress, these researchers introduced low-temperature combustion method to fabricate a highly crystalline Cu: NiO_x-compact layer at 150 ℃ with a work function of 5.3 eV compared to sol-gel processed (> 400 ℃) [159]. Moreover, combustion-processed-Cu:NiO_x exhibited higher electrical conductivity than that of high temperature-sintered film by almost two fold. The PSCs fabricated with the configuration of ITO/Cu:NiO_x/$CH_3NH_3PbI_3$/C_{60}/bis-C_{60}/Ag delivered a record efficiency of 17.74% at the time of report [94].

Furthermore, heavily doped metal oxide semiconductor as charge transporting layers in planar PSCs were also incorporated with large active-area (> 1 cm^2). These devices achieved a high-certified efficiency (> 15%) and better stability under continuous light-soaking for 1000 h [160]. The author employed heavily p-doped $Ni_xMg_{1-x}O$ and n-doped TiO_x as HTM and ETM, respectively, which displayed better charge transporting capability and minimized resistive losses, as confirmed by transient photocurrent and photo-voltage decay analysis. The improved performance was attributed to the efficient charge carrier collection and inhibited charge accumulation at the interface of HTM/$CH_3NH_3PbI_3$/ETM heterojunction. To overcome the limitations of the small FF, low J_{sc}, and hysteresis further modification with Mg in HTL/ETL was documented by Li et al. [127]. The Mg-doped NiO_x-HTL was applied in PSCs through sputtered-magnesium doping at low oxygen partial pressure. The p-i-n PSCs sandwiched by $MgNiO_x$-HTLs and PCBM/ZnMgO-ETLs obtained a PCE of 18.5%. On the other hand, the downwards shift *vs.* vacuum energy level in terms of V_B and V_C of perovskite has positive impact on the charge carrier management, in particular, the band energy alignments were beneficial for HTMs and ETMs to collect photo-generated holes and electrons with less energy loss, respectively. Recently, the low processing temperature (150 ℃), high crystallinity, homogeneity, optical transparency and high electrical conductivity has been widely reported with Cu-doped NiO_x film [94]. In this scenario, the proper amount of Cu doping in NiO_x film delivered high hole transport with a low resistance and reduce trap states, thus large FF and high J_{sc} values [73]. The PSCs consisting Cu-doped NiO_x-HTMs showed better improvement in PCE from 17.8% to 20.5%. Moreover, Chen et al. documented the stability of the encapsulated PSCs based on Cs:NiO_x HTLs stored for a period of 80 days [83]. The devices retained 90% of the initial PCE (19.35%) at ambient environment as depicted in Fig. 8b. However, a slow decay was observed due to the exposure of perovskite in air and moisture during the testing period. The high stability of the Cs:NiO_x devices further confirming the superior chemical stability of inorganic HTLs and substantial cathode interfacial layer [7,13,161]. Here, we summarized the best PSCs based on NiO_x-HTMs with their photovoltaic parameters in Table 2.

In comparison, all architectures follow the same charge transporting rate. However, the mesoporous PSCs show higher recombination rates [162]. On the other hand, the planar PSCs are suitable for the field of flexible solar cells because they do not need high annealing

Table 1
Photovoltaic parameters of the NiO-based PSCs as a function of thickness using ALD, PLD, sputtering, and spin-coated techniques. These parameters were taken with the permission from references [121,130,131,134,135].

	Atomic layer deposition [121]			
NiO-layer thickness (nm)	V_{oc} *(V)*	J_{sc} *(mA cm^{-2})*	*FF (%)*	*(%)*
205	1.049	18.74	60.6	11.80
5	1.026	19.19	62.0	12.16
7.5	1.041	18.79	60.8	11.63
10	1.046	16.90	58.0	9.860
5	1.046	17.56	56.0	9.840
7.5 **(Annealed NiO)**	1.040	21.37	71.8	15.52
	Pulsed-laser deposition [130]			
Oxygen pressure [mTorr]	V_{oc} *(V)*	J_{sc} *(mA cm^{-2})*	*FF (%)*	*(%)*
10	0.980	18.60	65.0	11.80
200	1.070	17.70	77.0	14.40
500	1.080	16.10	75.0	13.00
900	1.050	15.80	74.0	12.30
Film thickness [nm] (at partial O_2 pressure of 200mTorr)	V_{oc} *(V)*	J_{sc} *(mA cm^{-2})*	*FF (%)*	*(%)*
100	1.030	19.20	78.0	15.30
180	1.080	17.80	80.0	15.30
250	1.050	15.60	80.0	13.00
340	1.030	14.30	80.0	11.80
	Magnetron-sputtering deposition [131]			
NiO-layer thickness (nm)	V_{oc} *(V)*	J_{sc} *(mA cm^{-2})*	*FF (%)*	*(%)*
6.0	0.96	15.25	57.0	8.44
8.0	0.96	17.72	59.8	10.2
10	1.00	17.40	61.0	10.7
12	0.92	15.40	48.0	6.80
14	0.94	16.10	43.0	6.40
	Spin-coated deposition [134,135]			
NiO-layer thickness (nm)	V_{oc} *(V)*	J_{sc} *(mA cm^{-2})*	*FF (%)*	*(%)*
5.0	1.00	16.23	51.6	8.39
20	1.05	18.68	64.8	12.71
55	1.09	18.07	69.6	13.71
90	1.09	17.93	73.8	14.42
110	1.07	15.92	73.7	12.55
10	0.88	20.01	63.0	11.11
15	0.90	19.11	73.0	12.63
20	0.94	19.24	76.0	13.65
25	0.95	18.64	68.0	12.05
30	0.90	18.32	68.0	11.21

temperature. Additionally, n-i-p heterojunction exhibit good performance in terms of shorter diffusion length of hole than that of electron due to a larger effective mass of hole [2,163]. Whereas, planar p-i-n PSCs are helpful to reduce hysteresis with stable efficiency. Moreover, the trends of generation and recombination of charge carrier in PSCs were shown in Fig. 9a. The charge generation, separation and extraction processes take place from (1) to (3) which are desirable dynamics to get high performance in a PSCs. To manage efficient charge collection, these processes should be much faster than the recombination rate (undesirable) occurred from (4) to (7). To get further optimization and improvement in photovoltaic parameters, it is very important to understand the time scale and charge carrier kinetics occurring at different interfaces in PSCs.

The above sections described a systematic approach to the performance of PSCs incorporated with NiO_x-HTMs. The key factors include: the band gap alignment, efficient charge carrier extraction, high conductivity and deposition engineering across the whole device. We represented the efficiency tree with the best performance efficiency obtained with NiO_x-HTMs in different PSCs layout as depicted in Fig. 9b.

4. Cost assessment

Although boosting of PSCs efficiency is very essential, the cost evaluation of various raw materials and their manufacturing technologies are equally important. The capital, material and overhead costs analyses of PSCs have already been well documented in recent review articles [164–166]. In this section we will only focus on the assessment of materials, transparent conductive electrode, and charge transporting layers, perovskite layer, and counter electrode. In this regard, the cost analysis data for PSCs incorporated with NiO_x and conventional PSCs were taken from the literatures [149,150,167–169]. Conventional device was considered for the functional unit analysis, where spiro-OMeTAD as HTM and Au as back contact were used. The use of raw material for cleaning, fabrication of different thin films and sealing of the PSCs were extracted from various reported sources as described in Table 3 [170–172]. Regardless of the device architectures, all high efficiency PSCs so far employed small areas of 0.1 cm^2. As such a small device size is prone to induce measurement errors, a mandatory cell area of > 1 cm^2 is required for certified PCEs to be recorded in the standard of NREL. The total approximated cost of ~ 1 m^2 module for conventional PSCs was set to be ~ 1800/USD and ~ 800/USD for NiO_x-HTM based devices, respectively [7,172,173]. It is clear from Fig. 10 and Table 3 that above 50% of the total raw material cost is from organic-HTMs and the gold/silver back contact. Plainly, the first issue needs to be resolved is to develop an advanced fabrication technique to minimize waste of materials [174]. The ITO/FTO glasses are the most expensive parts of PSCs [175]. In scale-up processes of these substrates will significantly lower the module efficiency due to increase resistance [176]. Only few alternatives such as metal nanowire to these transparent electrodes were reported [177–179]. The second issue to be addressed is the expensive back metal electrode, which is usually gold or silver. Gold is precious while silver degrade the perovskite layer [180,181]. In this concern, the use of aluminum, nickel, copper and carbon were reported as suitable counter electrodes for high performance and stable PSCs [73,133,140,149,150,182]. Particularly, the carbon electrodes are pleasurable for low temperatures and scalable printing processes. However, the efficiency of carbon electrode-based devices must be improved just to catch up with that of current devices. Furthermore, the data illustrate that the organic-HTMs such as spiro-OMeTAD and PTAA are 23–57 times expensive compared to gold which will limit their industrial commercialization. The incorporation of additives such as LiTFSI in these organic HTMs limit the long-term stability of PSCs as well. In this scenario, the NiO_x-HTMs has successfully been employed in PSCs to replace the organic-HTMs with better stability at low cost.

5. Stability of NiO-based PSCs

The advancement in PCEs and areas of solar cell modules is rapidly increasing, the long-term stability of PSCs is still lag behind practical applications. In addition to considerable research aimed at maximizing efficiency, several studies have been demonstrated the degradation of PSCs [183–185]. It is widely reported that the stability issues of PSCs mainly result from the ambient environment, and from layers adjacent to the perovskite [186]. The typically adjacent layers (organic-HTLs or ETLs) and additives also limit the long-term stability [187,188]. One of the problems associated with spiro-MeOTAD is its macro-and micro-pin-holes which facilitate the inward and outward diffusion of gas species, thus cause PSCs to degrade [189]. The most widely used ionic dopant is LiTFSI to obtain pin-holes free spiro-OMeTAD. However, this dopant is hygroscopic and the absorption of moisture is the main cause for the instability. Also, it has been reported that the 4-tert-butylpyridine commonly added to spiro-MeOTAD to improve its compositional

Table 2
Photovoltaic parameters summary of PSCs based on NiO_x-HTMs with different architectures (M; represents mesoporous devices incorporating mesoporous scaffold (mp) of NiO, TiO_2, or Al_2O_3, P; denotes planar devices with compact (cp) layer of NiO or TiO_2, Psk; used for perovskite layer).

Type	Architecture	V_{oc} (V)	J_{sc} (mA cm^{-2})	FF (%)	(%)	Ref.
M	FTO/cp-NiO/mp-NiO/Psk/PCBM/Al	0.83	4.90	35.0	1.50	[61]
M	ITO/cp-NiO/mp-NiO/Psk/PC_{61}BM/BCP/Al	1.04	13.24	69.0	9.51	[60]
M	FTO/mp-NiO (sol-gel)/Psk/PCBM/Au	0.882	16.27	63.5	9.11	[56]
M	ITO/cp-NiO/mp-NiO/Psk/PCBM/BCP/Al	0.96	19.8	61.0	11.6	[123]
M	FTO/cp-NiO/mp-Al_2O_3/Psk/PCBM/BCP/Ag	1.04	18.0	72.0	13.5	[119]
M	FTO/cp-TiO_2/mp-TiO_2/mp-NiO/Psk/Carbon	0.89	18.2	71.0	11.4	[149]
M	FTO/cp-TiO_2/mp-TiO_2/mp-ZrO_2/mp-NiO/Psk/Carbon	0.965	20.4	72.0	14.2	[139]
M	FTO/cp-TiO_2/mp-TiO_2/mp-ZrO_2/mp-NiO/Psk/Carbon	0.917	21.36	76.0	14.9	[150]
M	FTO/cp-TiO_2/mp-TiO_2/mp-Al_2O_3/mp-NiO/Psk/Carbon	0.915	21.62	76.0	15.03	[141]
P	ITO/cp-NiO_x/Psk/PCBM/BCP/Al	0.92	12.43	68.0	7.80	[62]
P	ITO/cp-NiO_x (oxidized)/Psk/PCBM/BCP/Al	0.90	13.16	65.0	7.75	[155]
P	(TCO-free) Au: NiO/Psk/C_{60}/BCP/Al	1.02	13.04	77.0	10.24	[124]
P	FTO/cp-NiO/Psk/PCBM/Al	0.786	14.2	65.0	7.26	[125]
P	ITO/cp-NiO/Psk/PCBM/Al	1.05	15.4	48.0	7.60	[132]
P	FTO/cp-NiO/Psk/PCBM/BCP/Au	1.10	15.17	59.0	9.84	[118]
P	FTO/cp-NiO_x/Psk/PCBM/Ag	1.09	17.93	74.0	14.42	[146]
P	ITO/cp-Cu: NiO (sol-gel)/Psk/PC_{61}BM/C_{60}/Ag	1.11	18.75	72.0	14.98	[142]
P	ITO/cp-Cu: NiO (combustion)/Psk/C_{60}/bis-C_{60}/Ag	1.05	22.23	76.0	17.74	[94]
P	ITO/cp-NiO/Psk/PCBM/LiF/Al	1.06	20.2	81.3	17.3	[130]
P	PET/ITO/cp-NiO_x/Psk/C_{60}/bis-C_{60}/Ag	0.997	20.66	70.5	14.53	[122]
P	ITO/cp-NiO_x/Psk/C_{60}/bis-C_{60}/Ag	1.03	21.80	78.4	17.60	[122]
P	ITO/cp-NiO_x-PEDOT/Psk/PCBM/Ag	1.02	19.4	70.0	14.11	[157]
P	ITO/cp-NiO_x/Psk/ZnO/Al	1.01	21.0	76.0	16.1	[137]
P	FTO/cp-NiMgLiO/Psk/PCBM/Ti(Nb)O_x/Ag	1.072	20.21	74.8	16.2	[160]
P	ITO/cp-NiMgO/Psk/PCBM/ZnMgO/Al	1.078	21.3	79.0	18.5	[127]
P	FTO/cp-Cs: NiO_x/Psk/PCBM/ZrAcac/Ag	1.120	21.77	79.3	19.35	[83]
p	FTO/cp-Cu: NiO_x/Psk/PCBM/ZrAcac/Al	1.12	23.07	77.5	20.50	[73]
P	FTO/cp-TiO_2/Psk/NiO_x/Ni	0.77	17.88	53.0	7.28	[57]

uniformity can dissolve PbI_2 and decompose the perovskite layer [190–192].

In this regard, inorganic transporting layers have been documented with high stability when used in PSCs compared to organic charge carrier materials. Here we will aimed on the contribution of NiO_x-HTMs in high stable PSCs. The stability of unsealed PSCs in perovskite/silicon tandem cell for 1000 h under continuous maximum power point tracking (MMPT) has been demonstrated by Bush et al. [193]. The improvement in V_{MMP} was attributed to the favorable interface and valance band alignment between NiO_x and perovskite. On the other hand, decreasing J_{MMP} value was caused by the lack of an edge seal or pinholes in the ITO layer. This issue was controlled through packaging through the industry-standard encapsulation process. The sealed cells were further subjected to the damp heat test as described in the International Electrotechnical Commission (IEC) design qualification testing protocol 61215 for "Crystalline Silicon Terrestrial Photovoltaic (PV) Modules". After the encapsulation, J_{MMP} remained constant throughout the course of the damp heat test and the module withstand 85 °C and 85% relative humidity for 1000 h with no more than 10% degradation in performance, indicating that the packaging successfully addressed

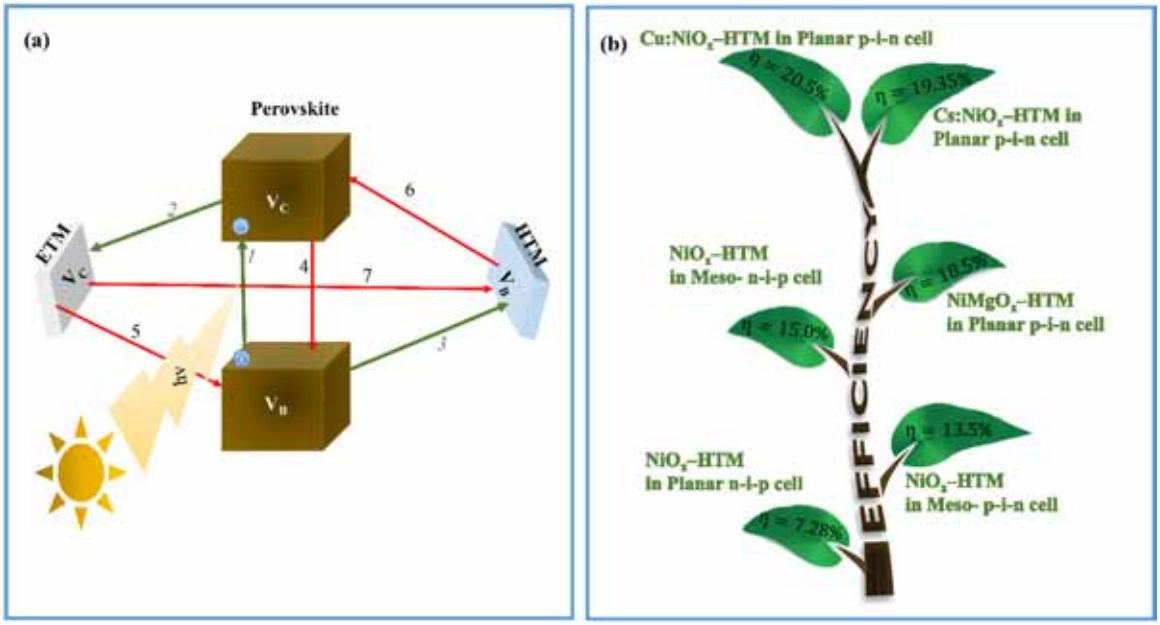

Fig. 9. (a) Pictorial representation of charge carrier transfer processes in PSCs. (b) Efficiency tree of PSCs incorporated with NiO_x-HTMs.

Table 3
Cost estimation of raw materials used in a PSC module of ~ 1 m^2 with 70% active area. Data's were collected in accordance with references [169,172].

Raw material	Qty	Price/USD	Contribution to total cost (%)	Remarks
ITO/FTO glass	1 m^2	766		Processing cost
Ethanol	32.85 ml	4.60	43.0600	of ITO/FTO is
DI water	32.72 ml	0.003		included
HCL solution	04.67 ml	1.8204		
Blocking layer				Post deposition
$TiCl_4$	19.16 ml	7.339	0.0066	and cleaning for
Ethanol	32.85 ml	4.60		100 nm thin
DI water	32.72 ml	0.003		layer
ETM layer				For 250 nm thick
TiO_2 paste	49.5 g	41.12	0.02291	mesoporous layer
Perovskite layer				Typically, for
PbI_2	1.38 g	4.26	0.003811	300 nm
DMF	2.98 ml	0.5502		perovskite layer
CH_3NH_3I	0.143 g	0.49		
IPA	14.29 ml	1.538		
HTM layer				For 200 nm thick
Organic-HTMs	0.850 g	603.65	33.973	HTM
Chlorobenzene	10.67 ml	5.9		
Back contact				For 100 nm thick
Au	1.65 g	330	18.392	layer
Sealing				Tape on both
3 M Tape	61.7 g	22.32	0.012	sides is included
PET		0.03		

potential problems such as pinholes in the ITO and an improper edge sealing [193]. Additionally, the HTL properties such as density, uniformity, hydrophobicity, and vulnerable reactivity with water can affect the cell durability. It has been confirmed by various research groups that the NiO_x-HTM layer as the outermost layer, despite having a good hole extraction affinity, could play as a surface barrier for water and oxygen diffusion. In this context, the durability of the PSCs with spiro-OMeTAD/Ag and NiO_x/Ni was traced at 25 °*C* ambient atmosphere with 28 ± 2% moisture [133]. Devices incorporated with NiO_x/Ni showed a stable PCEs for two months while the same structure with spiro-OMeTAD/Ag was completely out of efficiency by just 12 days. It was confirmed that the deposition of compact and very dense layer of NiO_x were pleasurable to control the diffusion of water molecules which cause degradation in perovskite and state-of-the-art organic HTMs. In addition to the intrinsic strong physical properties of the NiO_x layer, the strong surface mechanical properties such as scratching, indentation, and wear resistance can protect the perovskite layer against mechanical damages as well.

Furthermore, the NiO_x-based PSCs also exhibited better air stability compared with conventional PEDOT:PSS-based devices [135]. The degradation of PEDOT:PSS-based devices is due to the acidic and hygroscopic nature of such organic HTMs that damage the transparent conductive oxide electrodes and the adjacent moisture-sensitive perovskite [134]. Nonetheless, the intrinsic stability of perovskite material is a major concern regarding the long-life of PSCs. The NiO nanoparticles (NPs) composite in the $MAPbI_3$ layer has been implemented in PSCs and showed air stability over 60 days due to the strong chemical interaction between $MAPbI_3$ and NiO NPs as evidenced by the XPS spectra analysis [194]. The red-shift of Pb 4f peaks in $MAPbI_3$-NiO NPs composite showed the electrostatic interaction or covalent Pb-O bond formation in the contact area of the perovskite structure with NiO nanoparticles. This trend was consistent with increasing binding energy for the more electronegative oxide than the iodide ligand [195]. Furthermore, the iodide ligand worked as a link between Pb^{2+} and Ni^{2+} and helped in the formation of Ni-I bond (Fig. 11a). These crosslinking behaviors between neighboring grains in the perovskite structure contributed in the stability improvement [196]. The similar phenomena was described by Lin et al. [197] for the interfacial redox reaction occurred between PbI_2 and NiO_{nc}. The author further commented that the interfacial reactions induce iodine substitution by O in the formation of perovskite. The substituent hole-doping effect, like $MAPbI_{3-2x}O_x$ might function as a link to influence the charge and thus modify the J_{sc} and large FF of the solar cell as depicted in Fig. 11b.

Furthermore, the replacement of organic-HTMs by NiO_x was also helpful for investigating the influence of n-type materials (Lanthanum-doped $BaSnO_3$ *vs.* TiO_2) on the photostability for long-term measurements (~ 100 h) because organic-HTMs can degrade the PV performance by morphological deformation, metal diffusion and movable additives which will make it difficult to test photostability for long-term tests [198]. Moreover, carbon based PSCs with NiO_x-HTMs have been proven to possess better long-term stability than conventional cells with metal back contact [199,200]. Liu et al. showed the relatively better stability of sealed devices at constant light soaking [201]. The improved

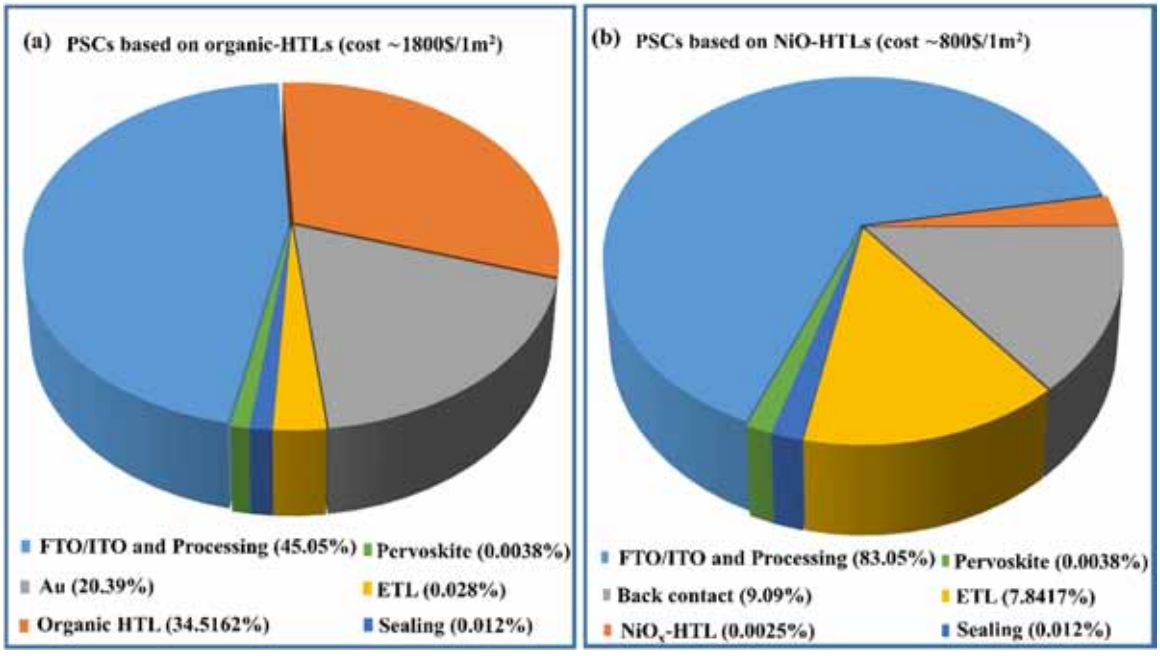

Fig. 10. Pie charts illustrate the cost-breakdown for PSCs incorporated with (a) organic-HTMs (b) NiO_x-HTMs.

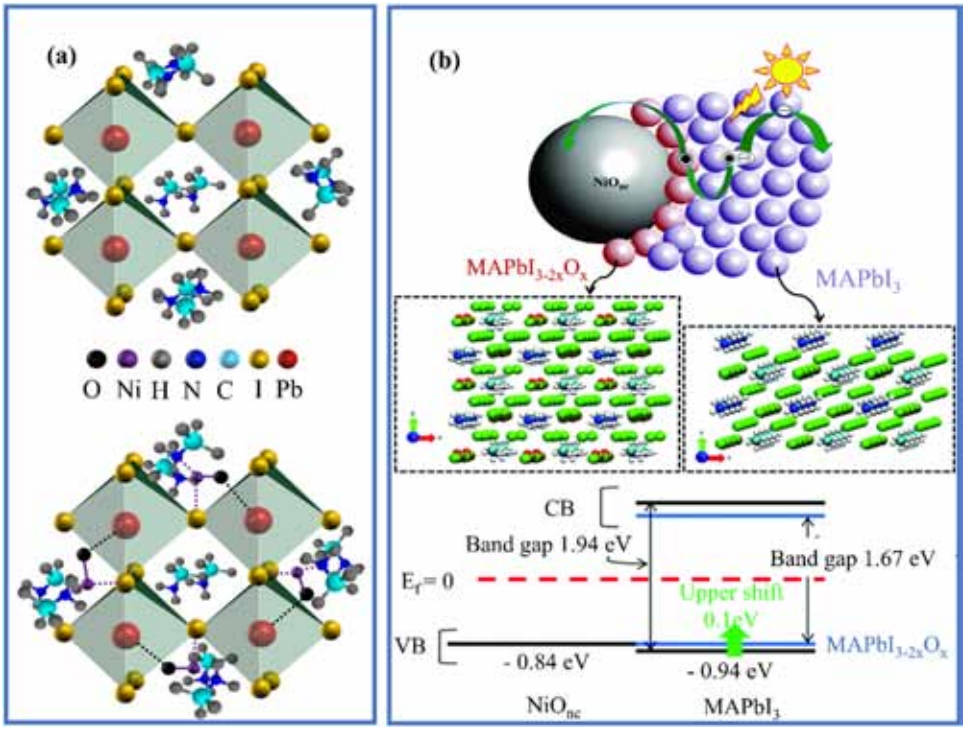

Fig. 11. (a) The 3D crystal structures of pristine $MAPbI_3$ (up) and $MAPbI_3$-NiO composite (down) where dash-lines indicate the Ni-N, Ni-I, NiO-N and Ni-O-Pb bonds. (b) Schematic replacement of two iodine atoms with one O atom accompanied by the upper shift in the valance band (VB) of the photoactive perovskite which indicates a facilitated hole injection from perovskite to NiO_{nc}. Reprinted with the permission from references [190,193].

stability was attributed to the hydrophobic property of carbon materials and a thick perovskite layer used, which might induce a slow degradation. In addition, the NiO nanosheets provided superior charge collection and prolonged charge lifetime. However, during the test, the photocurrent dropped significantly at the first 50 h. This problem was dealt by Cao et al. with mesoscopic scaffold of NiO/carbon in PSCs which showed almost constant J_{sc} value for 1000 h under ambient conditions [141]. This performance was attributed to reduce interfacial charge recombination in quadruple-layer mesoscopic PSCs which was entirely constructed with inorganic metal oxides in combination with carbon back contact by fully printable techniques. Similarly, 2D-nanosheets of NiO-HTMs with carbon electrode in PSCs maintained over 80% of its initial PCE [140]. Although, the stability of NiO_x with carbon back contact is higher, there is a huge gap in PCEs between the carbon-based devices and conventional PSCs. Improving the conductivity and interfacial contact between the carbon electrode and charge-selective layers will further boost the PCEs of PSCs with low production cost. Additionally, the extrinsic stability of PSCs can also be dealt with all metal oxide transporting layers. The possible resistance to the degradation mechanisms when using inorganic charge transporting materials may be due to (1) the resistance to the adsorption of oxygen/water (2) complete coverage of the perovskite film by inorganic-HTMs/ETMs, thus providing sufficient protection (3) These protections will further stop the chemical reaction between the counter electrodes (Al, Ag or Au) and the perovskite, and exposure to the ambient environment.

In total, the enhancement of long-term stability of PSCs will not only depend on the optimization of photoactive perovskite but also on the selection of stable HTMs and device structures to achieve high reproducibility and stability for scale-up production. The best device stability with NiO_x-HTMs were listed in Table 4. The low-cost and suitable stable materials such as all inorganic-transporting layers, NiO_x-HTMs, Ni, Cu and NiO_x-HTMs with carbon are promising alternatives to unstable organic charge transporting materials and expensive noble metals. Furthermore, an appropriate encapsulation method is also beneficial to cover the whole cells from degradation. However, for long-term stability measurements, a standard protocol should be adopted in order to understand degradation mechanisms and to compare different lab-scale methods.

6. Conclusions and future outlook

The emergence of PSCs has arouse exciting developments in the investigation of new HTMs and their variety of materials selection in device engineering. The high performance of PSCs relies on the choice of organic-HTMs, but their tedious synthetic processes, high purity, UV-sensitivity, low hole mobility, poly-dispersity, instability, and the risk of crystallization during heat exposure, needs to be addressed for their wide scale application. In this regard, we have summarized recent developments of NiO_x-HTMs being explored in PSCs, including the synthetic and fabrication methods, and their corresponding photovoltaic performances. As compared to their organic counterparts, the low production cost and high stability of NiO_x-HTMs render them most promising materials for large-scale application. Further enhancing the performance of NiO_x-HTMs in PSCs appears to be the key issue. It is concluded from the above survey that a successful NiO_x-HTM should have the following properties.

(i) The high p-type conductivity of NiO_x-HTM is required to get sufficient hole mobility and a suitable V_B level, which can result in improved performance. In this aspect, the introduction of nickel vacancies (Ni^{+3}) by extrinsic dopants with more shallow acceptor levels are pleasurable to increase the hole mobility and tunable V_B position.

(ii) The V_B of NiO_x-HTM should be matched with that of perovskite to extract and transmit hole efficiently. However, it is not so simple because it mystifies energy and free energy. In this regard, the actual description of the driving force is the difference between the Fermi level of the NiO_x-HTM and that of the holes in the perovskite under illumination. The lower charge carrier recombination rate should be maintained by enhanced hole collection from perovskite to NiO_x-HTM. This trend is observed with different V_{oc} values in well-aligned energetic levels between HTM and light active absorber [203]. The interfacial dipoles and chemical interactions at the surface of NiO_x-HTM/perovskite play a significant role to minimize trap states, recombination and energy losses, and thus

Table 4
Long-term stability test for PSCs incorporated with NiO_x-HTMs (Psk; represents perovskite layer, cp; describes the compact conducting layers either in planar devices or mesoporous devices, mp; denotes mesoporous scaffold layers in mesoporous devices, MPPT; maximum power point tracking).

Device	Time (h)	Light/dark	Temperature (℃)	Humidity (%)	Operation	Sea-ling	Performance	Ref.
ITO/cp-NiO_x/Psk/ZnO/Al	1440	Dark	25	Air (30–35)	J-V scan	No	~ 90%	[13]
FTO/cp-NiO_x/Psk/PCBM: PEI/Ag	1500	Dark	RT	Air (70)	J-V scan	Yes	> 90%	[202]
ITO/cp-NiO_x/Psk/C_{60}/bis-C_{60}/Ag	720	Dark	RT	Air	J-V scan	Yes	93%	[122]
FTO/cp-NiO_x/Psk/PCBM/Ag	150	Light	RT	Air (45–56)	J-V scan	No	> 80%	[135]
ITO/cp-NiO/Psk/LiF/$PC_{60}BM$/SnO_2/ZTO/ITO/LiF/Ag	1000	Light	35	Air (40)	MPPT	No	~ 100%	[193]
FTO/cp-NiMgLiO/Psk/PCBM/Ti(Nb)O_x/Ag	1000	Light	RT	Air	J-V scan	No	> 90%	[7]
FTO/cp-Cs: NiO_x/Psk/PCBM/ZrAcac/Ag	1680	Light	RT	Ar- box	J-V scan	Yes	~ 98%	[83]
FTO/cp-TiO_2/mp-TiO_2/mp-ZrO_2/mp-NiO/Psk/Carbon	250	Light	50	N_2-box	MPPT	Yes	60%	[201]
FTO/cp-TiO_2/mp-TiO_2/mp-ZrO_2/mp-NiO/Psk/Carbon	360	Dark	RT	Air (40)	J-V scan	Yes	> 80%	[140]
FTO/cp-TiO_2/mp-TiO_2/mp-Al_2O_3/mp-NiO/Psk/Carbon	1000	Dark	RT	Air (40)	J-V scan	No	> 80%	[141]
FTO/cp-TiO_2/mp-TiO_2/Psk-NiO (composite)/Au	1440	Light	25	Air (45–50)	J-V scan	No	~ 90%	[194]
FTO/cp-TiO_2/Psk/NiO_x/Ni	1440	Light	25	Air (30)	J-V scan	No	100%	[133]
ITO/cp-$BaSnO_3$/Psk/NiO/Au	1000	Light	RT	Air	MPPT	Yes	93%	[198]

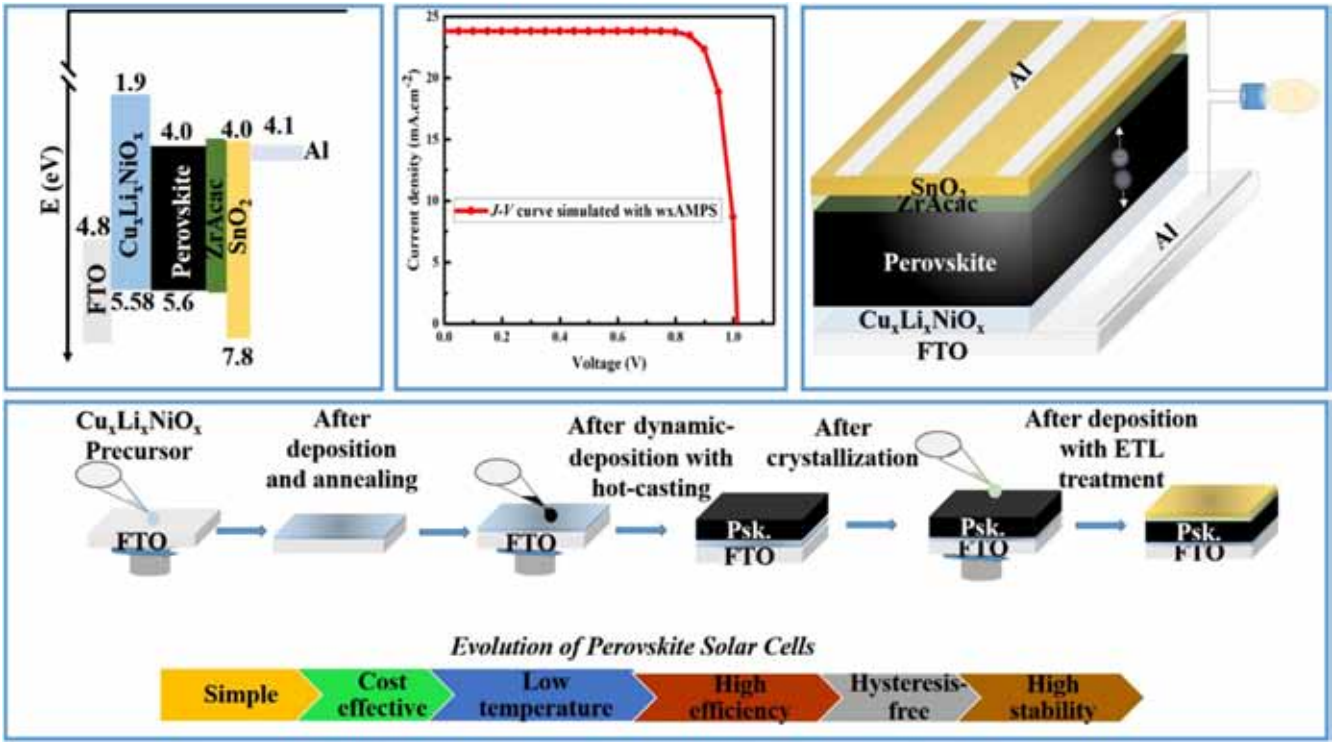

Fig. 12. Probable future device configuration for high efficiency, low-cost and stable PSCs.

encourage the essential driving force for hole injection.

(iii) High transparency in the visible and near infra-red region is pleasurable to minimize energy losses, especially, for tandem solar cell applications.

(iv) A compact and pinhole-free layer of NiO_x-HTM is needed to inhibit direct contact (shunting paths) of the perovskite with the front or back contacts. The incorporation of a thick NiO_x-HTM layer can minimize such shunting paths, but it should have enough conductivity and transparency to overcome the resistance and photon losses, respectively.

(v) The deposition methods for NiO_x-HTM layer needs to be optimized in terms of suitable solvent which does not damage the perovskite.

For the future outlook, it is worth notable that all highly efficient PSCs have been incorporated with PCBM as ETLs. Obviously, these ETLs are not only expensive but also hydrophilic in nature, which will severely impact the long-term stability of PSCs. Additionally, the valance band position of PCBM (5.8–6.04 eV) is not suitable to block photo-generated hole effectively which will further increase the charge recombination rate. However, the formation of induced-dipole by PCBM/perovskite interface is one of the helpful effects in controlling the ions migration in perovskite and thus deliver hysteresis-free PSCs. We strongly believe that it is possible to achieve high PCEs through the rational designing of NiO_x-HTMs, interfacial band alignment, optimization of doping and processing conditions, and reducing recombination losses together with suitable selection of perovskite. Therefore, it will be of great significance if we construct such PSCs which compose of all metal oxide-charge transporting materials and display high stability with negligible hysteresis at MPPT. Additionally, the approach of device engineering through energy band position alignment and modified deposition technique will provide large-scale manufacturing at low cost production with commercial viability [204,205]. Our group propose a scalable device configuration based on engineering the band gap alignment, modification of materials involved, and new deposition technique as shown in Fig. 12. Briefly, the proposed device is considered pleasurable for both intrinsic and extrinsic stability. The intrinsic instability is dealt with the stable perovskite such as (2D/3D) HOOC $(CH_2)_2NH_3)_2PbI_4$/$MAPbI_3$ perovskite, while extrinsic instability

with $Cu_xLi_xNiO_x$-HTL and SnO_2-ETL [206,207]. The incorporation of 2D/3D has already been yielded PCEs up to 12.9% in a carbon-based architecture, and 14.6% in spiro-OMeTAD-based cells with TiO_2 as ETL for each devices [206]. The $10 \times 10\,cm^2$ solar modules by printable process delivered 11.2% stable efficiency over 10,000 h with zero loss in performances measured under controlled standard conditions. However, the author documented that the PSCs based on carbon were annealed at 400 ℃ which will cause more stress and deformation, while spiro-OMeTAD devices showed instability due to the hygroscopic lithium salt and pin-holes in spiro-MeOTAD film which form channels to facilitate the inward and outward diffusion of gas species. Additionally, the use of TiO_2-ETLs in devices might also degrade the perovskite layer under UV illumination. In another literature the combination of ZnO-ETLs with NiO-HTLs in PSCs displayed stability up to 60 days [158]. However ZnO reacts with perovskite, causing instability due to the basic nature of ZnO. The thermal decomposition of the perovskite film is driven by acid-base chemistry at the ZnO/$MAPbI_3$ interface. Deprotonation of the MA^+ by the ZnO surface leads to the formation of MA and PbI_2. The basic hydroxyl groups from the ZnO surface further accelerate the decomposition process. More acidic metal oxides such as SnO_2 can produce perovskite films with better thermal stability. In this scenario, the layout of FTO/$Cu_xLi_xNiO_x$/2D-3D perovskite/SnO_2/Al will further increase the efficiency and stability with low production cost because carbon-based PSCs delivered lower efficiency while expensive spiro-OMeTAD delivered instability. On the other hand, the deposition of SnO_2-ETM has the capability to extract electrons and block holes effectively [208]. In addition, this ETM could reduce the diffusion of counter electrodes into perovskite which is one of the major reasons for device degradation. Thus the efficient charge carrier extraction and low recombination rate will further increase the FF and J_{sc}. The implementation of these promising materials are more attractive for further investigations to get stable PSCs with scalable low-cost production. It will also provide pathways to replace prohibitively expensive organic charge carrier transporters that have been widely used.

Acknowledgements

This work is supported partially by National Natural Science Foundation of China (Grant nos. 51772096, 51372082, 51402106 and 11504107), Beijing Natural Science Foundation (L172036), Joint Funds of the Equipment Pre-Research and Ministry of Education (6141A020225), National High-tech R&D Program of China (863 Program, No. 2015AA034601), Par-Eu Scholars Program, Beijing Municipal Science and Technology Project (Z161100002616039), the Fundamental Research Funds for the Central Universities (2016JQ01, 2017ZZD02) and the NCEPU "Double First-Class" Graduate Talent Cultivation Program.

References

[1] V. Roiati, et al., Energy Environ. Sci. 7 (6) (2014) 1889.
[2] G. Xing, et al., Science 342 (6156) (2013) 344.
[3] M.A. Green, et al., Nat. Photon 8 (7) (2014) 506.
[4] A.M. Elseman, et al., ACS Sustain. Chem. Eng. 4 (9) (2016) 4875.
[5] M.M. Rashad, et al., Opt. - Int. J. Light Electron Opt. 127 (20) (2016) 9775.
[6] A.M. Elseman, et al., Mater. Sci. Semicond. Proc. 66 (2017) 176.
[7] W. Chen, et al., Science 350 (6263) (2015) 944.
[8] A. Kojima, et al., J. Am. Chem. Soc. 131 (17) (2009) 6050.
[9] J.-H. Im, et al., Nanoscale 3 (10) (2011) 4088.
[10] H.-S. Kim, et al., Sci. Rep. 2 (2012) 591.
[11] W.S. Yang, et al., Science 348 (6240) (2015) 1234.
[12] N.J. Jeon, et al., Nature 517 (7535) (2015) 476.
[13] J. You, et al., Nat. Nanotechnol. 11 (1) (2016) 75.
[14] X. Wang, et al., Nano Lett. 17 (8) (2017) 4831.
[15] S. Sajid, et al., Nano-Micro Lett. 10 (3) (2018) 51.
[16] H. Zhou, et al., Science 345 (6196) (2014) 542.
[17] Y. Wu, et al., Nat. Energy 1 (11) (2016) 16148.
[18] N.-G. Park, J. Phys. Chem. Lett. 4 (15) (2013) 2423.
[19] Y.-F. Chiang, et al., Phys. Chem. Chem. Phys. 16 (13) (2014) 6033.
[20] D. Song, et al., J. Phys. Chem. C 119 (40) (2015) 22812.
[21] Z. Zhang, et al., Sol. Energy Mater. Sol. Cells 163 (2017) 250.
[22] Z. Zhang, et al., RSC Adv. 5 (127) (2015) 104606.
[23] A.E. Shalan, et al., Nanofibers as promising materials for new generations of solar cells, in: A. Barhoum, et al. (Ed.), Handbook of Nanofibers, Springer International Publishing, Cham, 2018, p. 1.
[24] A.M. Elseman, et al., ACS Appl. Mater. Interfaces 10 (14) (2018) 11699.
[25] W.S. Yang, et al., Science 348 (6240) (2015) 1234.
[26] M.A. Green, Prog. Photovolt.: Res. Appl. 23 (9) (2015) 1202.
[27] M. Saliba, et al., Science 354 (6309) (2016) 206.
[28] M. Saliba, et al., Energy Environ. Sci. 9 (6) (2016) 1989.
[29] W.S. Yang, et al., Science 356 (6345) (2017) 1376.
[30] N.J. Jeon, et al., J. Am. Chem. Soc. 136 (22) (2014) 7837.
[31] B. Xu, et al., Adv. Mater. 26 (38) (2014) 6629.
[32] Y. Liu, et al., Adv. Mater. 28 (3) (2016) 440.
[33] F. Zhang, et al., J. Mater. Chem. A 3 (48) (2015) 24272.
[34] J. Zhang, et al., Adv. Energy Mater. 6 (2016) 13.
[35] M. Cheng, et al., Nano Energy 30 (2016) 387.
[36] K. Rakstys, et al., J. Mater. Chem. A 5 (17) (2017) 7811.
[37] B. Xu, et al., Chem 2 (5) (2017) 676.
[38] D. Bi, et al., Nat. Energy 1 (2016) 16142.
[39] B. Cai, et al., Energy Environ. Sci. 6 (5) (2013) 1480.
[40] Y.S. Kwon, et al., Energy Environ. Sci. 7 (4) (2014) 1454.
[41] S. Ryu, et al., Energy Environ. Sci. 7 (8) (2014) 2614.
[42] Y. Zhang, et al., RSC Adv. 6 (110) (2016) 108888.
[43] Z. Yu, et al., RSC Adv. 7 (44) (2017) 27189.
[44] H.C. Liao, et al., Adv. Energy Mater. 6 (2016) 16.
[45] X. Jiang, et al., Sci. Rep. 7 (2017).
[46] K. Kranthiraja, et al., Adv. Mater. 29 (2017) 23.
[47] C.-H. Chiang, et al., Energy Environ. Sci. 10 (3) (2017) 808.
[48] Y. Rong, et al., Adv. Energy Mater. 5 (2015) 20.
[49] Y. Wu, et al., Energy Environ. Sci. 7 (9) (2014) 2934.
[50] P. Cui, et al., Sol. RRL 1 (2) (2017) 1600027.
[51] Z. Zhang, et al., Sol. Energy 122 (2015) 97.
[52] D. Wei, et al., J. Mater. Chem. A 5 (4) (2017) 1406.
[53] D. Song, et al., J. Mater. Chem. A 4 (16) (2016) 6091.
[54] T. Wang, et al., Sci. Chin. Mater. 59 (9) (2016) 703.
[55] P. Qin, et al., Nat. Commun. 5 (2014) 3834.
[56] Z. Zhu, et al., Angew. Chem. 53 (46) (2014) 12571.
[57] B.A. Nejand, et al., ACS Appl. Mater. Interfaces 7 (39) (2015) 21807.
[58] J.H. Im, et al., Nat. Nanotechnol. 9 (11) (2014) 927.
[59] J.Y. Jeng, et al., Adv. Mater. 25 (27) (2013) 3727.
[60] K.C. Wang, et al., Sci. Rep. 4 (2014) 4756.
[61] H. Tian, et al., ChemSusChem 7 (8) (2014) 2150.
[62] J.Y. Jeng, et al., Adv. Mater. 26 (24) (2014) 4107.
[63] M.-H. Li, et al., J. Mater. Chem. A 3 (17) (2015) 9011.
[64] Y. Xia, et al., Adv. Mater. 15 (5) (2003) 353.
[65] A. Morsali, et al., Inorg. Chim. Acta 362 (10) (2009) 3427.
[66] H. Yang, et al., J. Alloy. Compd. 459 (1–2) (2008) 98.
[67] S. Lany, et al., Phys. Rev. B 75 (24) (2007) 241203.
[68] K.H. Zhang, et al., J. Phys.: Condens. Matter 28 (38) (2016) 383002.
[69] Z. Liu, et al., J. Mater. Chem. A 5 (14) (2017) 6597.
[70] J.W. Jung, et al., Adv. Mater. 27 (47) (2015) 7874.
[71] Z. Yang, et al., Nano Energy 22 (2016) 328.
[72] A. Rajagopal, et al., J. Phys. Chem. Lett. 7 (6) (2016) 995.
[73] S. Yue, et al., Energy Environ. Sci. 10 (12) (2017) 2570.
[74] W. Chen, et al., Adv. Energy Mater. (2017).
[75] G. Natu, et al., ACS Appl. Mater. Interfaces 4 (11) (2012) 5922.
[76] M.-H. Liu, et al., Opt. Express 24 (22) (2016) A1349.
[77] G. Li, et al., Adv. Sci. 4 (12) (2017) 1700463.
[78] D. Ginger, N. Greenham, Phys. Rev. B 59 (16) (1999) 10622.
[79] N. Dharmaraj, et al., Mater. Sci. Eng.: B 128 (1–3) (2006) 111.
[80] K. Zhang, et al., Nanotechnol 19 (15) (2008) 155605.
[81] A.C. Gandhi, et al., RSC Adv. 6 (3) (2016) 2079.
[82] M.T. Greiner, et al., Nat. Mater. 11 (1) (2012) 76.
[83] W. Chen, et al., Adv. Energy Mater. 7 (19) (2017) 1700722.
[84] F. Al-Agel, Mater. Lett. 100 (2013) 115.
[85] E. Clementi, et al., J. Chem. Phys. 47 (4) (1967) 1300.
[86] M.M. Rashad, et al., Appl. Phys. A 117 (2) (2014) 877.
[87] P. Jeevanandam, Ranga Rao, NISCAIR-CSIR India 2012 (2012) 586.
[88] L.G. Teoh, K.-D. Li, Mater. Trans. 53 (12) (2012) 2135.
[89] Z. Zhu, et al., Angew. Chem. 126 (46) (2014) 12779.
[90] A.G. Merzhanov, J. Mater. Chem. 14 (12) (2004) 1779.
[91] M. Epifani, et al., J. Eur. Ceram. Soc. 27 (1) (2007) 115.
[92] X. Yu, et al., Proc. Natl. Acad. Sci. USA 112 (11) (2015) 3217.
[93] S. Bai, et al., Adv. Energy Mater. 4 (6) (2014) 1301460.
[94] J.W. Jung, et al., Adv. Mater. 27 (47) (2015) 7874.
[95] C.-.Y.H. Xiao-Ning Liao, Qiao-Ling Wang, Feng-Yi Chin. Chem. Soc., 56, p. 475.
[96] L. Wang, et al., RSC Adv. 3 (45) (2013) 23290.
[97] G.J. d.A.A. Soler-Illia, et al., Chem. Mater. 11 (11) (1999) 3140.
[98] N. Srivastava, P. Srivastava, Phys. E: Low-Dimens. Syst. Nanostruct. 42 (9) (2010) 2225.
[99] M. Ghosh, et al., J. Mater. Chem. 16 (1) (2006) 106.
[100] K.G. Chandrappa, et al., Mater. Corros. 63 (5) (2012) 445.
[101] M. Leskelä, M. Ritala, Thin Solid Films 409 (1) (2002) 138.
[102] T.S. Yang, et al., J. Vac. Sci. Technol. A: Vac. Surf. Films 23 (4) (2005) 1238.
[103] S. Rozati, S. Akesteh, Mater. Charact. 58 (4) (2007) 319.

[104] I. Sta, et al., Thin Solid Films 555 (2014) 131.
[105] C. Brinker, et al., Thin Solid films 201 (1) (1991) 97.
[106] H. Wang, et al., Electrochem. Commun. 18 (2012) 92.
[107] J.E. Mahan, Physical Vapor Deposition of Thin Films, Wiley-VCH, 2000, p. 336 (ISBN 0-471-33001-9).
[108] M.A. Herman, H. Sitter, Molecular Beam Epitaxy: Fundamentals and Current Status, Springer Science & Business Media, 2012.
[109] Y. Zhao, et al., Vacuum 103 (2014) 14.
[110] X. Xia, et al., Sol. Energy Mater. Sol. Cells 92 (6) (2008) 628.
[111] C. Luyo, et al., Sens. Actuators B: Chem. 138 (1) (2009) 14.
[112] C. Lampert, et al., Sol. Energy Mater. 14 (3–5) (1986) 161.
[113] F. Ferreira, et al., Solid State Ion. 86 (1996) 971.
[114] B. Subramanian, et al., Phys. B: Condens. Matter 403 (21) (2008) 4104.
[115] M.-S. Wu, et al., Electrochim. Acta 54 (2) (2008) 155.
[116] L. Soriano, et al., Phys. Rev. B 75 (23) (2007) 233417.
[117] Z. Zhu, et al., Angew. Chem. 126 (46) (2014) 12779.
[118] J. Cui, et al., ACS Appl. Mater. Interfaces 6 (24) (2014) 22862.
[119] W. Chen, et al., Energy Environ. Sci. 8 (2) (2015) 629.
[120] A.S. Subbiah, et al., J. Phys. Chem. Lett. 5 (10) (2014) 1748.
[121] S. Seo, et al., Nanoscale 8 (22) (2016) 11403.
[122] H. Zhang, et al., ACS Nano 10 (1) (2016) 1503.
[123] K.C. Wang, et al., ACS Appl. Mater. Interfaces 6 (15) (2014) 11851.
[124] W.C. Lai, et al., Adv. Mater. 28 (17) (2016) 3290.
[125] A.S. Subbiah, et al., J. Phys. Chem. Lett. 5 (10) (2014) 1748.
[126] M. Liu, et al., Nature 501 (7467) (2013) 395.
[127] G. Li, et al., Adv. Sci. 4 (2017) 12.
[128] T. Dutta, et al., J. Appl. Phys. 108 (8) (2010) 083715.
[129] Y.A.K. Reddy, et al., J. Mater. Sci. Technol. 29 (7) (2013) 647.
[130] J.H. Park, et al., Adv. Mater. 27 (27) (2015) 4013.
[131] K.-C. Wang, et al., ACS Appl. Mater. Interfaces 6 (15) (2014) 11851.
[132] L. Hu, et al., ACS Photonics 1 (7) (2014) 547.
[133] B. Abdollahi Nejand, et al., ACS Appl. Mater. Interfaces 7 (39) (2015) 21807.
[134] H. Zhang, et al., ACS Nano 10 (1) (2015) 1503.
[135] X. Yin, et al., J. Mater. Chem. A 3 (48) (2015) 24495.
[136] X. Yin, et al., J. Power Sources 329 (2016) 398.
[137] J. You, et al., Nat. Nano 11 (1) (2016) 75.
[138] Y. Hou, et al., Adv. Mater. 28 (25) (2016) 5112.
[139] Z. Liu, et al., J. Mater. Chem. A 3 (47) (2015) 24121.
[140] D. Guo, et al., Sol. Energy Mater. Sol. Cells 159 (2017) 518.
[141] K. Cao, et al., Nano Energy 17 (2015) 171.
[142] J.H. Kim, et al., Adv. Mater. 27 (4) (2015) 695.
[143] A. Nattestad, et al., Nat. Mater. 9 (1) (2010) 31.
[144] X.-H. Chan, et al., J. Electrochem. Soc. 158 (7) (2011) H733.
[145] M.D. Irwin, Proc. Natl. Acad. Sci. USA 105 (8) (2008) 2783.
[146] X. Yin, et al., J. Mater. Chem. A 3 (48) (2015) 24495.
[147] P. Docampo, et al., Nat. Commun. 4 (2013) 2761.
[148] J. Burschka, et al., Nature 499 (7458) (2013) 316.
[149] Z. Liu, et al., Dalton Trans. 44 (9) (2015) 3967.
[150] X. Xu, et al., Nano Lett. 15 (4) (2015) 2402.
[151] Z. Liu, et al., J. Mater. Chem. A 5 (14) (2017) 6597.
[152] Sajid, et al., Chin. Phys. B 27 (1) (2018) 17305.
[153] H. Tian, et al., ChemSusChem 7 (8) (2014) 2150.
[154] V. Trifiletti, et al., ACS Appl. Mater. Interfaces 7 (7) (2015) 4283.
[155] W.C. Lai, et al., IEEE Trans. Electron Devices 62 (5) (2015) 1590.
[156] M. Xiao, et al., Angew. Chem. Int. Ed. 53 (37) (2014) 9898.
[157] I.J. Park, et al., J. Phys. Chem. C 119 (49) (2015) 27285.
[158] J. You, et al., Nat. Nanotechnol. 11 (2015) 75.
[159] J. He, et al., Sol. Energy Mater. Sol. Cells 62 (3) (2000) 265.
[160] W. Chen, et al., Science 350 (6263) (2015) 944.
[161] W. Chen, et al., Adv. Mater. 29 (2017) 16.
[162] V. Gonzalez-Pedro, et al., Nano Lett. 14 (2) (2014) 888.
[163] S.D. Stranks, et al., Science 342 (6156) (2013) 341.
[164] L. Qiu, et al., Mater. Today Energy (2017).
[165] M. Cai, et al., Adv. Sci. 4 (2017) 1.
[166] N.L. Chang, et al., Progr. Photovolt.: Res. Appl. 25 (5) (2017) 390.
[167] N. Espinosa, et al., Energy Environ. Sci. 5 (1) (2012) 5117.
[168] U. Posset, et al., RSC Adv. 2 (14) (2012) 5990.
[169] S. Maniarasu, et al., Renew. Sustain. Energy Rev. 82 (2018) 845.
[170] S. Bilgen, et al., Energy Sources 26 (12) (2004) 1119.
[171] I. Dincer, Energy Sources 23 (1) (2001) 83.
[172] J. Gong, et al., Energy Environ. Sci. 8 (7) (2015) 1953.
[173] H.-C. Liao, et al., Adv. Energy Mater. 7 (8) (2017) 1601660.
[174] F. Ye, et al., Energy Environ. Sci. 9 (7) (2016) 2295.
[175] A. Binek, et al., ACS Appl. Mater. Interfaces 8 (20) (2016) 12881.
[176] M. Hambsch, et al., J. Mater. Chem. A 4 (36) (2016) 13830.
[177] D. Bryant, et al., Adv. Mater. 26 (44) (2014) 7499.
[178] F. Guo, et al., Nanoscale 7 (5) (2015) 1642.
[179] H. Sun, et al., Energy Environ. Sci. 8 (4) (2015) 1139.
[180] Y. Kato, et al., Adv. Mater. Interfaces 2 (2015) 13.
[181] S.-G. Li, et al., J. Mater. Chem. A 3 (17) (2015) 9092.
[182] J. Zhao, et al., Energy Environ. Sci. 9 (12) (2016) 3650.
[183] G. Niu, et al., J. Mater. Chem. A 3 (17) (2015) 8970.
[184] T.A. Berhe, et al., Energy Environ. Sci. 9 (2) (2016) 323.
[185] E.J. Juarez-Perez, et al., Energy Environ. Sci. 9 (11) (2016) 3406.
[186] T. Leijtens, et al., Nat. Commun. 4 (2013) 2885.
[187] Z. Hawash, et al., Chem. Mater. 27 (2) (2015) 562.
[188] M.-C. Jung, et al., Sci. Rep. 5 (2015) 9863.
[189] L.K. Ono, et al., J. Mater. Chem. A 3 (30) (2015) 15451.
[190] E.J. Juarez-Perez, et al., Chem. Mater. 28 (16) (2016) 5702.
[191] S. Wang, et al., Nano Lett. 16 (9) (2016) 5594.
[192] W. Li, et al., J. Mater. Chem. A 2 (33) (2014) 13587.
[193] K.A. Bush, et al., Nat. Energy 2 (4) (2017) 17009.
[194] Y. Wang, et al., Nano Energy 27 (2016) 535.
[195] A.P. Grosvenor, et al., Surf. Sci. 600 (9) (2006) 1771.
[196] X. Li, et al., Nat. Chem. 7 (9) (2015) 703.
[197] M.W. Lin, et al., Adv. Mater. Interfaces 3 (2016) 17.
[198] S.S. Shin, et al., Science 356 (6334) (2017) 167.
[199] A. Mei, et al., Science 345 (6194) (2014) 295.
[200] X. Li, et al., Energy Technol. 3 (6) (2015) 551.
[201] Z. Liu, et al., J. Mater. Chem. A 3 (47) (2015) 24121.
[202] H.C. Liao, et al., Adv. Energy Mater. 7 (2017) 8.
[203] M. Saliba, et al., Nat. Energy 1 (2) (2016) 15017.
[204] S. Yue, et al., Small 13 (2017) 19.
[205] A. Guerrero, et al., ACS Nano 6 (4) (2012) 3453.
[206] G. Grancini, et al., Nat. Commun. 8 (2017) 15684.
[207] Z. Zhu, et al., Adv. Mater. 28 (30) (2016) 6478.
[208] Q. Jiang, et al., Nat. Energy 2 (1) (2017) 16177.

Sajid Sajid received his bachelor's degree in Physics & Mathematics and Master's degree in Physics from Government Post Graduate College Charsadda and Kohat University of Science and Technology KPK, Pakistan, respectively. Recently, he is a PhD scholar at State Key Laboratory of Alternate Electrical Power System with Renewable Energy Sources, School of Renewable Energy, North China Electric Power University, Beijing 102206, China. His current research focuses on understanding mechanisms and fundamental properties of organometal halide perovskite and on developing scalable protocols for high-efficiency perovskite solar cells.

Ahmed Mourtada Elseman is an assistant professor (Post-Doctoral) at Department of Electronic and Magnetic Materials, Central Metallurgical Research & Development Institute (CMRDI), Egypt. He obtained his Ph.D. degree from Chemistry Department, Al-Azhar University, for perovskite solar cells in February 2017. He is a senior researcher at School of Renewable Energy, North China Electric Power University, China. His current research focuses on understanding mechanisms and fundamental properties of organometal halide perovskite and on developing scalable protocols for high-efficiency perovskite solar cells. He is member of Editorial Board at some journal.

Meicheng Li is the Director of New Energy Materials and PV Technology Center, and the Vice Dean of the School of Renewable Energy, North China Electric Power University. He obtained his PhD at Harbin Institute of Technology in 2001. He worked in University of Cambridge as Research Fellow from 2004 to 2006. He won the Excellent Talents in the New Century by the ministry of education in 2006. His current research topic is the New Energy Materials and Devices, such as solar cells, lithium ion battery. Till now, he contributed more than 200 journal articles. He got almost more than 10 items of awards for the science and technology success. He is an executive fellow of the China Energy Society, fellow of Chinese Society for Optical Engineering.